Contribution of voltage-gated sodium channels to the b-wave of the mammalian flash electroretinogram

Deb Kumar Mojumder, David M. Sherry and Laura J. Frishman

College of Optometry, University of Houston, 505 J Davis Armistead Bldg, 4901 Calhoun Road, Houston, TX 77204-2020, USA

Voltage-gated sodium channels (Na_v channels) in retinal neurons are known to contribute to the mammalian flash electroretinogram (ERG) via activity of third-order retinal neurons, i.e. amacrine and ganglion cells. This study investigated the effects of tetrodotoxin (TTX) blockade of Na_v channels on the b-wave, an ERG wave that originates mainly from activity of second-order retinal neurons. ERGs were recorded from anaesthetized Brown Norway rats in response to brief full-field flashes presented over a range of stimulus energies, under dark-adapted conditions and in the presence of steady mesopic and photopic backgrounds. Recordings were made before and after intravitreal injection of TTX ($\sim$3 μM) alone, 3–6 weeks after optic nerve transection (ONTx) to induce ganglion cell degeneration, or in combination with an ionotropic glutamate receptor antagonist 6-cyano-7-nitroquinoxaline-2,3-dione (CNQX, 200 μM) to block light-evoked activity of inner retinal, horizontal and OFF bipolar cells, or with the glutamate agonist *N*-methyl-D-aspartate (NMDA, 100–200 μM) to reduce light-evoked inner retinal activity. TTX reduced ERG amplitudes measured at fixed times corresponding to b-wave time to peak. Effects of TTX were seen under all background conditions, but were greatest for mesopic backgrounds. In dark-adapted retina, b-wave amplitudes were reduced only when very low stimulus energies affecting the inner retina, or very high stimulus energies were used. Loss of ganglion cells following ONTx did not affect b-wave amplitudes, and injection of TTX in eyes with ONTx reduced b-wave amplitudes by the same amount for each background condition as occurred when ganglion cells were intact, thereby eliminating a ganglion cell role in the TTX effects. Isolation of cone-driven responses by presenting test flashes after cessation of a rod-saturating conditioning flash indicated that the TTX effects were primarily on cone circuits contributing to the mixed rod–cone ERG. NMDA significantly reduced only the additional effects of TTX on the mixed rod–cone ERG observed under mesopic conditions, implicating inner retinal involvement in those effects. After pharmacological blockade with CNQX, TTX still reduced b-wave amplitudes in cone-isolated ERGs indicating Na_v channels in ON cone bipolar cells themselves augment b-wave amplitude and sensitivity. This augmentation was largest under dark-adapted conditions, and decreased with increasing background illumination, indicating effects of background illumination on Na_v channel function. These findings indicate that activation of Na_v channels in ON cone bipolar cells affects the b-wave of the rat ERG and must be considered when analysing results of ERG studies of retinal function.

(Resubmitted 7 January 2008; accepted after revision 28 March 2008; first published online 3 April 2008)
Corresponding author L. J. Frishman: College of Optometry, University of Houston, 505 J Davis Armistead Bldg, 4901 Calhoun Road, Houston, TX 77204-2020, USA. Email: lfrishman@uh.edu

Neurophysiological studies of blockade of Na_v channels using tetrodotoxin (TTX) (Narahashi *et al.* 1964; Kao, 1966) in isolated mammalian retinal slice preparations or dissociated neurons have shown that these channels are prominent and functional in retinal ganglion cells (e.g. Lipton & Tauck, 1987; Skaliora *et al.* 1993) and in some types of amacrine cells (e.g. AII, A17, A18 and starburst amacrine cells; Boos *et al.* 1993; Feigenspan *et al.* 1998; Hartveit, 1999; Cohen, 2001). More recently, functional Na_v channels in isolated bipolar cells and bipolar cells in retinal slice preparations have been observed in several species: rat (Pan & Hu, 2000), goldfish (Zenisek *et al.* 2001), salamander (Ichinose *et al.* 2005; Ichinose & Lukasiewicz, 2007), ground squirrel (Saszik & DeVries, 2005) and

This paper has online supplemental material.

 DOI: 10.1113/jphysiol.2008.150755

human (Miyachi *et al.* 2006; Ohkuma *et al.* 2007). In the rat retina, functional Na_v channels were found in cone but not rod bipolar cells (Pan & Hu, 2000). Their absence from rod bipolar cells, suggests an additional postreceptoral divergence in physiological properties of rod *versus* cone circuits (Pan & Hu, 2000; Ma *et al.* 2005).

The activity of Na_v channels in bipolar cells has been shown recently to be modulated by ambient background illumination in the tiger salamander retinal slice (Ichinose & Lukasiewicz, 2007) where the Na_v channels contributed more to the bipolar cell response under low light conditions than high light conditions. The authors suggested that the Na_v channels in bipolar cells provide an additional retinal mechanism for adjusting sensitivity over a wide range of ambient illuminations. Another known mechanism of light adaptation involves switching circuits. For example under fully dark-adapted conditions, rod signals travel via rod bipolar cells (primary rod circuit) to inner retina. Under mesopic conditions, when rod bipolar cell responses saturate, rod signals can be relayed to the inner retina via a second rod circuit via gap junctions between rods and cones, and then via cone bipolar cells (Nelson *et al.* 1975; Nelson, 1977; Schneeweis & Schnapf, 1995; Guldenagel *et al.* 2001; Deans *et al.* 2002). A third rod circuit exists in which rods contact OFF- or ON-cone bipolar cells directly (Soucy *et al.* 1998; Tsukamoto *et al.* 2001; Protti *et al.* 2005; Tsukamoto *et al.* 2007). Because of the switching of circuits, the overall contribution of Na_v channels to light-evoked signal processing in the retina can be expected to vary with changes in ambient illumination.

In the present study we investigated the effects of light adaptation on retinal Na_v channel function *in vivo*, in the Brown Norway rat retina, using the electroretinogram (ERG). ERGs have been used extensively to study retinal activity as a function of the level of light adaptation (e.g. Green & Powers, 1982; Frishman & Sieving, 1995; Frishman *et al.* 1996; Wang *et al.* 2001; Naarendorp *et al.* 2001; Saszik *et al.* 2002*b*). Results have been interpreted based on known origins of ERG waves. For example, the major waves of the ERG, the a- and b-waves, have well-defined neuronal origins (e.g. Frishman, 2005, for review). a-waves originate primarily from photoreceptors, although more proximal cells in OFF pathways also contribute under some conditions (Bush & Sieving, 1994; Robson *et al.* 2003). The b-wave reflects mainly light-induced depolarization of ON bipolar cells (e.g. Xu & Karwoski, 1994; Robson & Frishman, 1995; Robson *et al.* 2004) but may be shaped by the activity of other cells, including Müller cells (Miller & Dowling, 1970; for review see Frishman, 2005), and under light-adapted conditions there are contributions from OFF bipolar, horizontal cells and more proximal cells (Sieving *et al.* 1994; Viswanathan *et al.* 1999). Oscillatory potentials (OPs) arise primarily from inner retinal activity, amacrine (Wachtmeister, 1998 for review), or ganglion cells (Rangaswamy *et al.* 2006).

Intravitreally injected TTX reduces the amplitude of smaller ERG components from inner retina such as the negative scotopic threshold response, (nSTR: monkey, Ahmed *et al.* 1999; rat, Bui & Fortune, 2004), the positive STR (pSTR) in rat, and photopic negative response (PhNR: monkey, Viswanathan *et al.* 1999), and also affects the amplitude and time course of the b-wave (rabbits, Dong & Hare, 2000; salamander, Awatramani *et al.* 2001), a finding that the authors attributed to inner retinal mechanisms. In rats TTX has been reported to attenuate the photopic b-wave but to hardly affect the maximum amplitude of the scotopic b-wave (Bui & Fortune, 2004; Li *et al.* 2005; Mojumder *et al.* 2007), raising the possibility of effects on cone but not rod bipolar cells, consistent with observations in single cell recordings of Pan & Hu (2000). Ganglion cell lesions have also been reported to attenuate the photopic b-wave, and the pSTR and nSTR) in rat retina (Bui & Fortune, 2004).

In the present study, the effects of TTX on the rat ERG were found to be related to background level. Consistent with previous observations in rats, the effect on b-waves was present in the cone bipolar cell, but not rod bipolar cell-mediated responses. Much of the TTX effect on b-waves could be localized to the cone bipolar cells themselves, regardless of background level. However, under mesopic conditions where the effects of TTX on the mixed rod–cone b-wave amplitude were greatest, evidence was found in ganglion cell lesion and pharmacological blockade studies for additional effects, possibly originating from spiking amacrine cells. In contrast to previous findings in rats (Bui & Fortune, 2004), ganglion cell lesions in the present study did not affect the amplitude of the b-wave significantly under any background conditions.

Methods

Subjects

Subjects were adult Brown Norway rats, 7 weeks to 6 months of age (Charles River Laboratories, Inc., Wilmington, MA, USA). Details of the number of rats used for each experiment are presented in Table 1, and as the table shows, specific experiments were generally done with rats of similar ages. The rats were reared and housed in a room with a 12 h light (< 40 lux)–12 h dark cycle. All animal procedures conformed to US Public Health Service and Institute for Laboratory Animal Research guidelines and were approved by the University of Houston Institutional Animal Care and Use Committee.

ERG recording

The recording setup was similar to that previously described for studies in mice (Saszik *et al.* 2002*b*). Animals

Table 1. Summary of pharmacological studies and age at time of ERG recordings

Drug treatment	Number of eyes	Number of rats	Ages
Flash ERG with incrementing backgrounds (before *versus* after TTX)	20	20	11–21 weeks
Transient background (before *versus* after TTX)	2	2	7–8 weeks
Determining cone-isolation protocol	16	16	13–21 weeks
Photopic *versus* cone-isolated photopic ERG	4	4	24–26 weeks
Cone-isolated ERG (before and after TTX)	14	14	15–19 weeks
NMDA + TTX	12	10	14–16 weeks
CNQX + TTX	6	4	14–16 weeks
Control *versus* ONTx	6	6	13–17 weeks
ONTx *versus* ONTx + TTX	6	6	16–18 weeks

were dark-adapted overnight and prepared for recording under red illumination (LED, $\lambda > 620$ nm). They were initially anaesthetized with an intramuscular injection of ketamine (86 mg kg^{-1}) and xylazine (6.5 mg kg^{-1}; both drugs from Vedco St Joseph, MO, USA) into the hamstring muscles. Immobilization was maintained with ketamine (43 mg kg^{-1}) and xylazine (3 mg kg^{-1}) every 45–60 min, via a subcutaneous needle fixed to the flank. Animals generally recovered after the sessions; however, after intravitreal injections of pharmacological agents in both eyes, they were killed using an intraperitoneal dose of sodium pentobarbital (100 mg kg^{-1}). Pupils were dilated to 5 mm in diameter with topical atropine (0.5%) and phenylephrine (2.5%). A drop of proparacaine hydrochloride (0.5%) was used for corneal anaesthesia. Rectal temperature was maintained between 36 and 37°C with an electrically heated blanket (CWE, Inc., Ardmore, PA, USA). The animal's head was held steady, in order to reduce noise originating from respiratory and other movements, using an aluminium head holder with a hole for the upper incisors. This head holder also served as the earth.

Recording sessions lasted 4–8 h. ERGs were recorded differentially between DTL fibre electrodes (Dawson *et al.* 1979) moistened with normal saline and placed on the two eyes. The stimulated eye was covered with a contact lens heat-moulded from ACLAR (Ted Pella, Inc., USA) and the non-stimulated eye, with an opaque plastic contact lens. Both lenses were placed over a cover of methylcellulose saline. The signals were amplified (DC to 300 Hz), digitized at 1 kHz with a resolution of 2 μV, and sent to the computer for averaging, display and storage, and subsequent analysis.

Stimuli for elicting ERGs

ERGs were recorded using brief full-field LED flashes (λ_{max}, 462 nm; –5.8 to 1.9 log sc td s) from darkness, and in the presence of steady backgrounds ranging from –1.7 to 2.3 log sc td (λ_{max}, 462 nm). This stimulus was similar to the one used and more fully described in Saszik *et al.* (2002*b*). Adapting backgrounds were described as being mesopic or rod-suppressing based on work of others (e.g. Toda *et al.* 1999; Wang *et al.* 2001; Naarendorp *et al.* 2001; Xu *et al.* 2003; Table 2). Steady backgrounds were present for 15–20 min before accepting ERG recording for analysis (Bui & Fortune, 2006). The intervals between flashes were adjusted so that the response returned to baseline before another stimulus was presented. For flash energies $\leq$ –2.8 log sc td s, intervals were 1.5 s; $>$ –2.8 and $\leq$ –1.2 log sc td s, 2 s; $>$ –1.2 and $\leq$ 1.3 log sc td s, 3 s and intervals between flashes of higher energy than 1.3 log sc td s were 4 s. Low amplitude responses such as the scotopic threshold response (STR) were averaged over many trials (40–60) and higher amplitude responses, over fewer trials (10–20). A digital 60 Hz notch filter was applied offline. Two other stimulus protocols, one for use of transient backgrounds, and one for isolation of cone-driven signals, are discussed in appropriate sections of Results.

Intravitreal injections

Injections were performed using a binocular operating microscope (×10 magnification) under dim red illumination ($\lambda > 620$ nm) to avoid light-adapting the rods. A small pilot hole was punctured ~0.5–1 mm behind the limbus using a 30G needle to facilitate subsequent penetration at 45 deg of the globe by a fine glass micropipette (tip ~20 μm) fixed on a 10 μl Hamilton microsyringe (Hamilton Company, Reno, NV, USA). The volume of the pharmacological agents injected was ~2 μl to ensure reproducibility, and avoid loss of the injectate and risk of local complications (Dureau *et al.* 2001). The injection was given slowly over 1 min to allow diffusion of the drug (Martin *et al.* 2003). All agents were diluted in balanced salt solution buffered close to pH 7.4. Drug concentrations (TTX, ~3 μM; *N*-methyl-D-aspartate (NMDA), 100–200 μM; 6-cyano-7-nitroquinoxaline-2,3-dione (CNQX) 200 μM) were selected and adjusted for an estimated vitreous chamber volume of 40 μl (Hughes, 1979; Dureau *et al.* 2001). After injection the ERG was monitored until the drug effects on the waveform were stable (approximately 45 min), and were found to remain so by comparing results for similar background conditions tested at varying

Table 2. Background conditions that were used

Background	Luminance (log sc cd m^{-2})	Illumination (log sc td)	Illumination ($Rh^* s^{-1}$ per rod)
Dark-adapted	—	—	—
Mesopic	–2	−0.7	29.5
Mesopic	–1	0.3	295.1
Mesopic	0	1.3	2951.2
Rod-suppressing	10	2.3	29 512

time points in different experiments. In fact, recovery from TTX takes days, and of the other drugs used, only NMDA effects have been observed to change about 12 h after intravitreal injection (DK Mojumder & LJ Frishman, unpublished observations).

Light calibration

Light calibration was done as previously described (Saszik *et al.* 2002*b*). The scotopic luminance was measured with a scotopically corrected photometer (International Light model IL1700, USA), and subsequently the luminance–time product for each of the single flash stimuli was derived, expressed in sc cd s m^{-2}, and converted to sc td s by multiplying by the pupillary area of 19.63 mm^2. Based on the study of Naarendorp *et al.* (2001), a flash of 1 sc td s should produce ∼147 photoisomerizations per second per rod ($Rh^* s^{-1}$ per rod) in the rat retina.

Data analysis

ERG b-wave amplitudes were measured at fixed times after the stimulus flash chosen to correspond to the b-wave peak times for the backgrounds and flash energies that were used. The hypothesis that there was no difference in the effects of background on the TTX-sensitive ERG amplitudes corresponding to b-wave times to peak was assessed by one-way analysis of variance (ANOVA; MATLAB, v7.01, statistical toolbox; The MathWorks, Inc., Natick, MA, USA). This was followed by *post hoc* analysis to evaluate if TTX-sensitive amplitudes produced by each background were different from one another. *t* tests, or paired comparison tests, were used for other comparisons as appropriate.

Unilateral optic nerve transection (ONTx)

The optic nerve was approached by a perilacrimal route using a modification of a technique previously described (Kermer *et al.* 2001). This approach, which excluded the globe from any surgical manipulation, was utilized to prevent the possibility of damage to the posterior ciliary blood vessels and those in the globe, which is a hazard for other approaches. The rat was anaesthetized with xylazine (86 mg kg^{-1}) and ketamine (8 mg kg^{-1}), and 0.5% proparacaine HCl was used as topical corneal anaesthesia. The animal's head was shaved and then cleaned with surgical spirit, povidine iodine solution (10%) and surgical spirit applied consecutively to maintain asepsis and antisepsis. The scalp skin was incised parasagittally close to the superior orbital border. Careful dissection spared both the superior orbital vein superficially and the frontal nerve under the deep fascia. Blunt dissection was performed through the periorbital fat. Posteriorly, the intraorbital lacrimal glands were identified and then the levator palpabrae superioris muscle was revealed subsequent to which the superior rectus was identified lying below and medial to it. These were retracted to expose the optic nerve covered by the retractor bulbi muscle, which was gently separated longitudinally. The optic nerve was gently pulled up, and its sheath was incised longitudinally (approx. 1 mm) using a keratome. A specially made blunt-tipped curved glass retractor was inserted through the sheath to lift the nerve away from the closely apposed posterior ciliary artery and vein (Sugiyama *et al.* 1999). The nerve was completely transected using Vannas scissors alongside the retractor approximately 2 mm from the sclera. Transection was confirmed using a silvered lens expressor behind the transected nerve and while transilluminating the optic nerve (see figure in online Supplemental material). Post-operatively the fundus was viewed under the operating microscope using a flat coverslip apposed on the cornea to ensure an intact blood column in the retinal blood vessels (Supplemental figure). Topical 1% atropine sulphate was used for post-operative cycloplegia. Neomycin and polymyxin B sulphates and bacitracin zinc ophthalmic ointment (AK-SPORE, Akorn; Abita Springs, LA, USA) was used on the wound site. The skin was sutured with 6-0 silk and dressed with neomycin and polymyxin B sulphates and bacitracin zinc ophthalmic ointment. The wound was administered broad spectrum antibiotic ointment and monitored closely daily for 7 days. The success of the procedure was verified immunohistologically in post mortem tissue, 3–6 weeks after ONTx and following ERG recording.

Immunohistochemistry

Animals and tissue preparation. Light-adapted adult rats (6 weeks to 6 months; $n = 7$) that had undergone ONTx 3–6 weeks earlier, followed by ERG recording, were used for immunohistochemical analysis of retinal ganglion cells. Animals were killed by injection of a lethal dose of pentobarbital (150–200 mg kg^{-1}) and the eyes were rapidly excised from the head. The corneas were slit open, the lens was expressed, and the eyes were immersed in 4% formaldehyde in 0.1 M cacodylate buffer (pH 7.4) for 24 h at 4°C. The eyes were rinsed in phosphate-buffered saline (PBS; pH 7.4), cryoprotected in 30% sucrose in PBS over-

Table 3. Primary antibodies and antisera

Antigen	Cell type labelled	Host	Dilution	Source	Reference
Neurofilament, 200 kDa	Ganglion cell and axons; Horizontal cell axons	Mouse	1 : 1000	Chemicon International, Temecula, CA, USA (Cat. no. MAB5266; clone N52)	Shaw & Weber (1983)
Brn-3a	Ganglion cell nuclei	Mouse	1 : 25	Chemicon International (Cat. no. MAB1585; clone 5A3.2)	Xiang *et al.* (1995)
Microtubule associated protein-1 (MAP-1)	Retinal ganglion cells	Mouse	1 : 300	Sigma-Aldrich, St Louis, MO, USA (Cat. no. M4278; clone HM-1)	Huber & Matus (1984)
Calretinin	Conventional and displaced starburst amacrine cells	Rabbit	1 : 1000	Chemicon International (Cat. no. AB148)	Winsky *et al.* (1989); Pasteels *et al.* (1990)
Calbindin	Horizontal and amacrine cells	Mouse	1 : 5000	SWANT, Bellinzona, Switzerland (Cat. no. 300)	Celio *et al.* (1990); Pasteels *et al.* (1990)
Choline acetyl transferase (ChAT)	Conventional and displaced starburst amacrine cells	Goat	1 : 100	Chemicon International (Cat. no. AB144P)	Ostermann *et al.* (1990); Voigt (1986)
Protein kinase C (PKC)	Rod bipolar cells	Rabbit	1 : 100	Calbiochem, EMD Biosciences, Inc., San Diego, USA (Cat. no. 539601)	Negishi *et al.* (1988); Haverkamp & Wässle (2000)
Vesicular glutamate transporter-1 (VGluT-1)	All photoreceptor and bipolar cell terminals	Guinea pig	1 : 1000	Chemicon International (Cat. no. AB5905)	Johnson *et al.* (2003); Sherry *et al.* (2003*a*)
Glial fibrillary acidic protein (GFAP)	Astrocytes and reactive Müller cells	Mouse	1 : 500	Chemicon International (Cat. no. MAB360; clone GA5)	Debus *et al.* (1983); Bignami & Dahl (1979); Björklund *et al.* (1985)

night at 4°C, embedded in OCT embedding medium (Tissue-Tek, Elkhart, IN, USA) and fast frozen in liquid nitrogen. Vertical frozen sections through the retinal layers were taken along the vertical meridian of the eyecup at a thickness of 10–12 μm and collected onto Superfrost Plus microscope slides (Fisherbrand, Fisher Scientific, Pittsburgh, PA, USA). Sections were stored at –20°C until use.

Antibodies and antisera. Well-characterized mouse monoclonal antibodies or rabbit polyclonal antisera were used as specific markers for different retinal neurons and glia. Details of primary antibodies are presented in Table 3. Secondary antisera were raised in goat and were specific for either mouse or rabbit immunoglubulins and conjugated to fluorescent dyes: Alexa Fluor-488 (dilution 1 : 200–1 : 500; Molecular Probes, Eugene, OR, USA) or Cy3 (dilution 1 : 200–1 : 500; Jackson ImmunoResearch Laboratories, West Grove, PA, USA).

Immunolabelling. Immunofluorescent labelling of frozen sections was performed as previously described (Sherry *et al.* 2003*a*,*b*, 2006; Mojumder *et al.* 2007). Sections were thawed, fixed in 4% paraformaldehyde for 10–15 min at room temperature to improve section adherence to the slide, rinsed, treated with 1–2% $NaBH_4$ to reduce autofluorescence, and rinsed again. Non-specific labelling was blocked using 10% normal goat serum, 5% bovine serum albumin, 0.5–1% fish gelatin and 0.1% Triton X-100 in PBS (blocker). Excess blocker was removed and the sections were incubated in a combination of primary antibodies diluted in blocker for 2 days at 4°C. The sections were rinsed, blocked for 30 min, and then incubated with a combination of secondary antibodies

for 30–45 min at room temperature. Sections were rinsed, coverslipped in a fade-retardant mounting medium containing 4′,6-diamidino-2-phenylindole (DAPI) (Vectashield, Vector Laboratories, Burlingame, CA, USA) and examined in the microscope.

To confirm the specificity of immunolabelling methods, sections were processed in the absence of primary antibodies or by substituting normal rabbit serum for rabbit polyclonal primary antisera. As appropriate, these treatments eliminated labelling. All antibodies and antisera were diluted in the appropriate blocker solution.

Imaging. Imaging was performed by conventional and confocal fluorescent light microscopy. For conventional fluorescence microscopy, greyscale images of immunolabelling were captured directly from the microscope. Image scale was calibrated and, if necessary, brightness and contrast were adjusted to highlight specific immunolabelling. For double and triple labelling experiments, matching images in the DAPI, Alexa Fluor-488 and Cy3 channels were captured and pseudocoloured blue, green, or red, respectively. Matching images in the different channels were overlaid using Adobe Photoshop 6.0 software (Adobe Systems, Inc., Mountain View, CA, USA) to compare localization of labelling.

Confocal images were acquired using a Leica TCS SP2 confocal microscope (Leica Microsystems, Exton, PA, USA). Images were captured using either ×20 (NA, 1.2), ×63 oil (NA, 1.32), or ×63 water immersion (NA, 1.2) objective lenses. Stacks of serial optical sections were collected at a step size of 0.3–0.6 μm step size. Bleed-through between the channels was removed by adjusting laser intensity and detector sensitivity and by sequentially imaging each fluorescent channel. The images shown are either projections of an image stack or are a single, representative optical section. Figures were prepared using Adobe Photoshop 6.0 software.

Results

Effects of TTX on the ERG b-wave depend upon the background illumination

Figure 1*A* shows typical ERGs recorded after intravitreal administration of TTX (grey traces), compared to those recorded before TTX for the same animal (black traces). Shown in this figure are responses to a saturating flash of energy 1.6 log sc td s, presented over a range of steady background illuminations. For this flash strength, the effects of TTX were greatest under mesopic conditions. A small reduction of the b-wave amplitude under dark-adapted conditions (more obvious in later figures) was replaced by a greater reduction when mesopic backgrounds were present (−0.7 and 0.3 log sc td). When backgrounds induced photopic (rod-saturating, 2.3 log sc td), or nearly photopic (1.3 log sc td) conditions, the reduction in b-wave amplitude was smaller than that observed under mesopic conditions.

The leading edge of the dark-adapted a-wave reflects the activity of rod photoreceptor at early times after a brief flash (up to 5 ms in humans and monkeys: Hood & Birch, 1990; Nusinowitz *et al.* 1995; Birch *et al.* 2002; Robson *et al.* 2003). a-waves from control ERGs and ERGs after TTX injection are shown on an expanded time scale in the lower set of traces in Fig. 1*A*. The leading edges were well aligned for all backgrounds for which there was a discernable a-wave, indicating no loss of rod photoreceptor sensitivity due to the injection. However, at 14–18 ms after the flash, the dark-adapted a-wave for a flash of 1.9 log sc td s was about 20% larger in eyes treated with TTX than in control recordings ($n = 9$; paired t test; $P < 0.05$). This occurred in the region where the a-wave was likely to be affected by postreceptoral influences (shaded area in plot inset in Fig. 1*A*) (Robson & Frishman, 1996; Robson *et al.* 2003). For lower flash energies increases in amplitude were not significant. An increase in the a-wave peak amplitude after TTX injection was previously described for the rabbit ERG (Dong & Hare, 2000).

The results in Fig. 1*A*, as well as most of those reported in this paper, were from animals that were tested first under dark-adapted conditions and then in the presence of incrementing backgrounds. It was therefore important to distinguish the specific effects of TTX for a particular background from potential time-related experimental effects due, for example, to time under anaesthesia, deterioration of the animal's physiological condition, or long-term effects of intravitreal drug administration.

To exclude the possibility of time-dependent effects, for two animals, the time between the dark-adapted and light-adapted conditions was shortened by using transient backgrounds. As illustrated in Fig. 1*B*, three equally spaced flashes (1.6 log sc td s) were presented so that the first one (from darkness) preceded the onset of a transient (1600 ms) mesopic background (0.3 log sc td), the second one occurred on the background, 1000 ms after its onset, and the third was presented 6100 ms after offset of the background. A large reduction in b-wave amplitude in an eye injected with TTX (grey lines) occurred only when the flash was presented on the background. After the background was turned off, the ERG (right hand column) quickly returned to an amplitude and time course similar to that recorded under dark-adapted conditions. ERGs recorded prior to TTX injection (black lines in Fig. 1*B*) have been superimposed on the post-TTX responses to illustrate the magnitude of the attenuation caused by TTX when the transient background was present. Similar findings occurred in both animals tested with this protocol, and for a flash energy of 1.3 also tested in the same two animals.

Effect of stimulus energy. Figure 2 shows typical effects of TTX for a range of stimulus energies presented under dark-adapted conditions and on steady backgrounds inducing mesopic and photopic levels of adaptation. Under dark-adapted conditions and photopic conditions the results of this study were similar to those previously described in the literature. TTX removed most of the inner retinal potentials in the dark-adapted ERG that occurred in response to low energy flashes (bottom five traces in the left-hand panel): the nSTR and the pSTR. For higher stimulus energies (1.3 and 1.6 log sc td s), TTX slightly reduced the b-wave amplitude. Under photopic conditions (2.3 log sc td), for all stimulus energies the b-wave was reduced by TTX. TTX also removed most of the PhNR, a potential of inner retinal origin, observed to be TTX-sensitive in monkeys (Viswanathan *et al.* 1999, 2000) and in Brown Norway rats (Li *et al.* 2005). Under mesopic conditions, not previously studied, the effects of TTX were surprisingly large. For the mesopic backgrounds of −0.7 log sc td and 0.3 log sc td, TTX

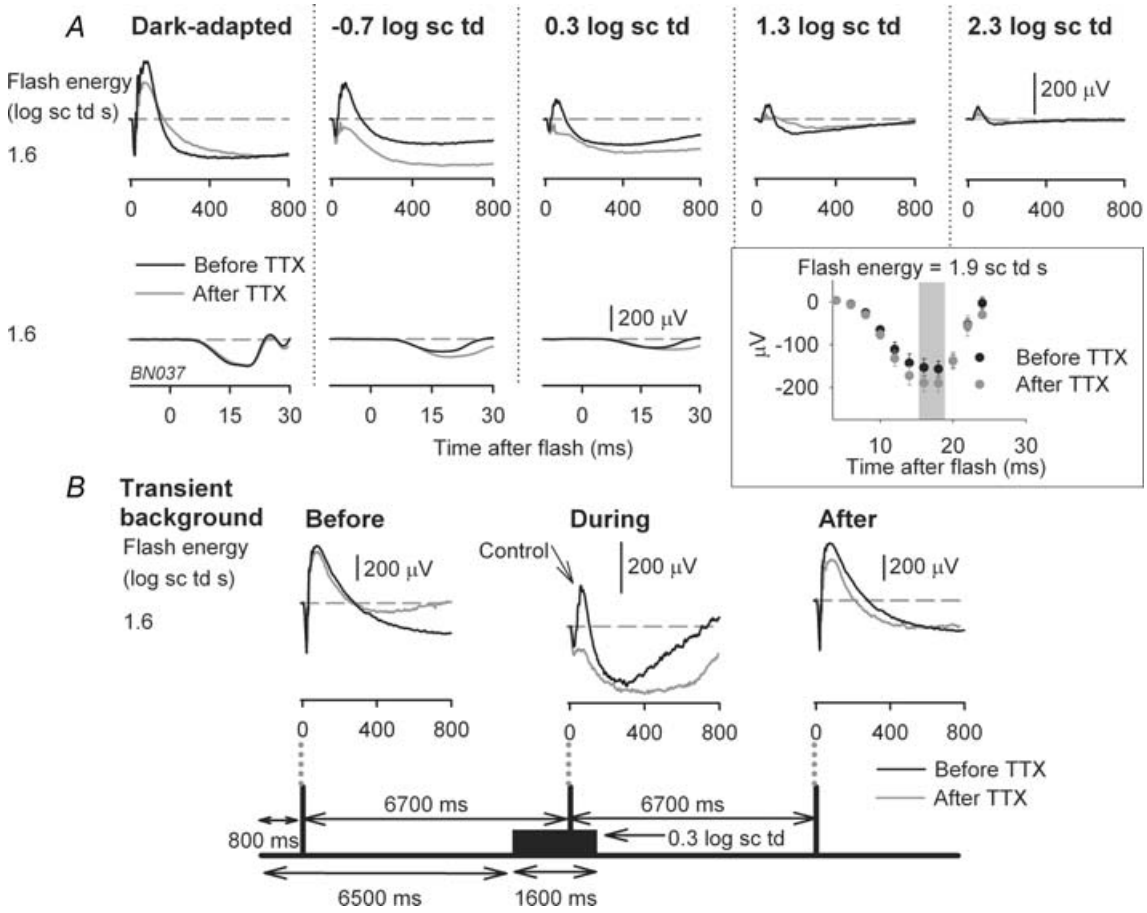

Figure 1. Effect of TTX on the electroretinogram (ERG) depends on background illumination
A, effect of intravitreal injection of TTX on the ERG response to a high energy flash (1.6 log sc td s) for background conditions ranging from fully dark-adapted (left) to photopic with a rod-suppressing background of 2.3 log sc td (right). Top row: superimposed ERG responses before (black traces) and after intravitreal injection of TTX (grey traces) in one subject. Bottom row: the leading edge of the a-wave on an expanded time scale. The inset shows the average dark-adapted ERG amplitudes (group mean ± S.E.M.) before (black circles) and after (grey circles) intravitreal injection of TTX ($n = 9$) measured at fixed times on the leading edge of the a-wave. The grey area indicates the times at which the increase in a-wave amplitude was statistically significant (paired t test; $P < 0.05$). *B*, effect of TTX on the ERG for high energy flash (1.6 log sc td) delivered before, during and after a transient background was presented. Schematic diagram at the bottom indicates the times for flash delivery relative to the onset and offset of a transient background of 0.3 log sc td (1600 ms duration) for a single subject. The flashes were spaced 6700 ms apart such that the second flash was delivered at 1000 ms after onset of the transient background. The corresponding ERG responses to stimuli of 1.6 sc td s recorded after TTX are indicated by the grey lines; the control responses before TTX are illustrated by the superimposed black lines. Comparison of the grey and black lines when the transient background was present indicates the extent of attenuation of the b-wave by TTX for that background condition.

caused a large attenuation of the b-wave that increased as stimulus energy was increased. The extent to which the traces became negative-going under mesopic conditions varied, with the traces in Fig. 2 at the more negative end of the range. TTX altered but did not eliminate oscillatory potentials (OPs); this feature was particularly obvious under mesopic conditions for stimulus energies of 1.3 and 1.6 log sc td s.

In order to quantify the effects of TTX, for each background condition, ERG amplitudes were measured at fixed times after the flash, corresponding to the time to peak of the b-wave. As shown in Fig. 3, the b-wave time to peak decreased with increasing stimulus energy and background illumination. Under dark-adapted conditions, measurements were made at 110, 65 and 50 ms after the flash, to capture changes in peak time as the stimulus energy was increased. The longest time to peak shortened to 80 ms when the background was −0.7 log sc td, and to 65 ms when it was 0.3 log sc td. Under photopic conditions (2.3 log sc td), the peak of the cone-driven b-wave occurred at 50 ms. These different times to peak were also appropriate for post-TTX records. Measurements of amplitude at fixed times were made from the baseline at 0 μV, and did not take into account the negative photoreceptor and inner retinal responses that formed the true baseline for the b-wave. This was done because the negative-going signals were affected by TTX in some cases, e.g. a-waves in Fig. 1*A*, and later in the response in some animals, as in Fig. 2, for mesopic backgrounds, and therefore were not easily quantified or modelled. The measurements at 50 and 65 ms sometimes included the later OPs on the leading edge of the b-wave, particularly when mesopic backgrounds were present. However, any contribution of the OPs to the large effects of TTX under mesopic conditions would have been small (see Figs 2 and 4).

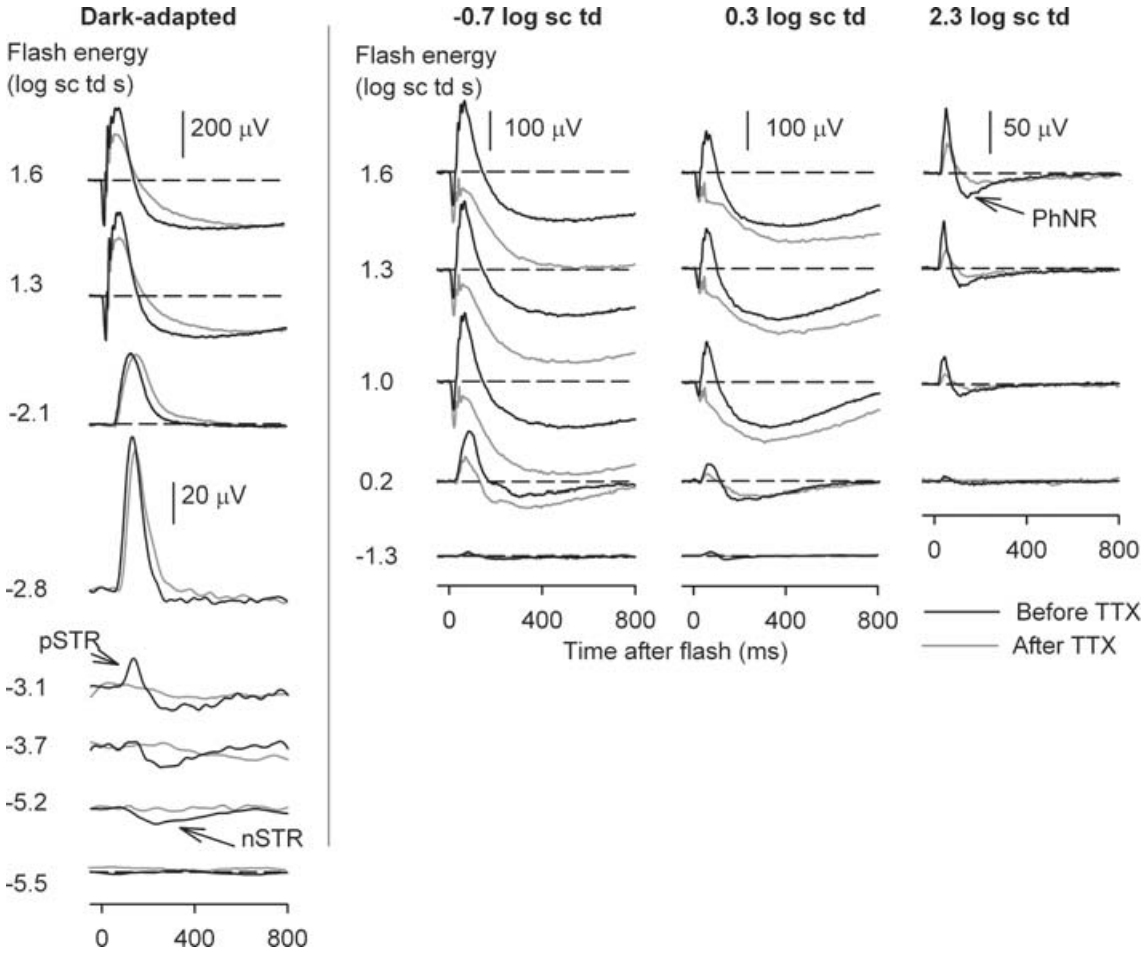

Figure 2. ERG responses to brief full-field flashes of increasing energy and incrementing background illumination

ERG responses for representative subjects to a range of increasing stimulus energies, from bottom to top, for four different background adaptation conditions (from left to right: dark-adapted, mesopic (−0.7 log sc td and 0.3 log sc td) and photopic (2.3 log sc td), before (black traces) and after TTX (grey traces). pSTR, positive scotopic threshold response; nSTR, negative scotopic threshold response; PhNR, photopic negative response.

As shown in Fig. 4 (top row, right-hand plot) for dark-adapted conditions, the ERG amplitude measured at 110 ms was not affected by TTX for flash energies below those that saturated the response, and above those (i.e. –2.0 log sc td s) for which a pSTR would normally be present in the response. The small, but significant, response attenuation for flash energies < -3.4 log sc td s ($P < 0.05$) was probably due to effects of TTX on the pSTR (Fig. 2, and in Bui & Fortune, 2004, their Fig. 7). Amplitudes measured at earlier times under dark-adapted conditions, 50 and 65 ms, on the rising edge of the b-wave (top row left and centre plots), were not affected by TTX up to the first saturation of the curve. Past the initial saturation, as stimulus energy was increased, TTX reduced the b-wave amplitude for each of the times analysed.

For the lower mesopic background of −0.7 log sc td, stimulus–response curves (Fig. 4, second row) showed two or three saturating limbs. TTX had no obvious effects on the small initial limb which was generated in response to the same very low stimulus energies that were used to generate the dark-adapted stimulus–response curve up to its saturation. In contrast, for all three time points, 50, 65 and 80 ms, attenuation of the b-wave was profound for the responses to higher energies.

The higher mesopic background (0.3 log sc td) (Fig. 4, third row) reduced sensitivity sufficiently for the very low stimulus energies no longer to be effective. For higher stimulus energies, TTX reduced b-wave amplitudes, and the reduction increased as stimulus energy was increased. Similar effects were seen for the photopic ERG (Fig. 4, bottom row, left).

The similarity of results across time points for the individual dark-adapted and mesopic conditions indicated that for analyses of further experiments, one time point common to all backgrounds, 50 ms, the only time used for the photopic condition, could be selected. For measurements at 50 ms, the TTX-sensitive ERG was derived for responses to a 1.0 and 1.6 log sc td s flash by subtracting the response after TTX from the control response (Fig. 4, bottom row, right). Two flash energies were selected for comparisons of TTX effects across background conditions to take account of the desensitization that occurred with increasing background illumination. For both flash strengths, the TTX-sensitive response was more than twice as large when the mesopic, – 0.7 log sc td, background was present than under any other conditions. The effect of TTX was also proportionally greater under mesopic conditions, than other background conditions, as will be shown in a later section (Fig. 14).

To determine whether TTX was affecting rod- or cone-initiated signals and their pathways selectively, the cone signals were isolated in the experiments described in the next section.

TTX reduced the amplitude of the cone-driven b-wave

Cone isolation. The stimuli (λ_{max}, 462 nm) used in these experiments affected mainly rods ($\lambda_{max} = \sim$500 nm) and

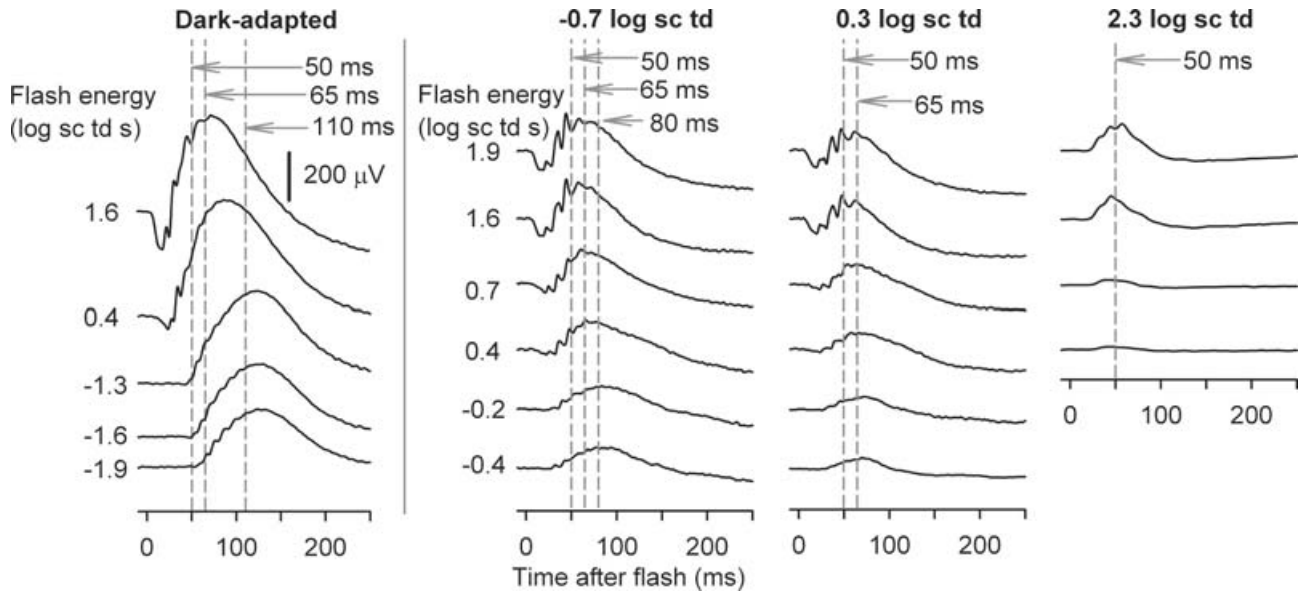

Figure 3. Criterion times corresponding to peak amplitudes of the b-waves for different background conditions and flash energies
ERG responses to brief full-field flashes of increasing energy, from bottom to top, over a range of incrementing background illumination commencing from the dark-adapted condition (left to right) for a representative subject (BN102). Vertical (grey dashed) lines indicate criterion times at which the peak amplitude of the b-wave was measured: 110, 80, 65 and 50 ms.

m-cones ($\lambda_{max} = \sim 510$ nm), and had a minimal effect on the UV cones ($\lambda_{max} = \sim 360$ nm) (Jacobs *et al.* 2001; Akula *et al.* 2003). Because of the overlapping rod and m-cone spectral sensitivity, it was not possible to use different wavelength stimuli to separate rod- and cone-driven responses. Therefore, as illustrated in Fig. 5, a cone-isolation protocol was used. The protocol was based on the well-established fact that cones recover more quickly than rods following suppression of photocurrents (Thomas & Lamb, 1999; Paupoo *et al.* 2000). In the present study, an initial conditioning flash (6.3 log sc td, 1 s duration) was used to suppress the rod photocurrent completely, but the cone currents to a lesser extent, as can be seen by the ERG response to the test flash during the conditioning flash in Fig. 5*A*. Probing with a test flash at incrementing time points gives the time course of recovery of the ERG, with responses at early time points after extinction of the conditioning flash being cone-driven, and responses at late time points, rod-driven as well (Nusinowitz *et al.* 1995; Lyubarsky *et al.* 1999, 2002; Friedburg *et al.* 2001; Robson *et al.* 2003). To extract the response to the test flash alone at each interstimulus interval (ISI), the response to the conditioning flash alone was subtracted from the records which contained both responses. The recovery of the cone-driven responses with increasing ISI for one rat eye can be seen in Fig. 5*A*. Note that the a-wave also recovered with increasing ISI (Fig. 5*B*, drawn on an expanded time scale). As shown in Fig. 5*B*, a-waves at 800–1200 ms after the conditioning flash were considerably smaller, characteristic of cone-driven a-waves

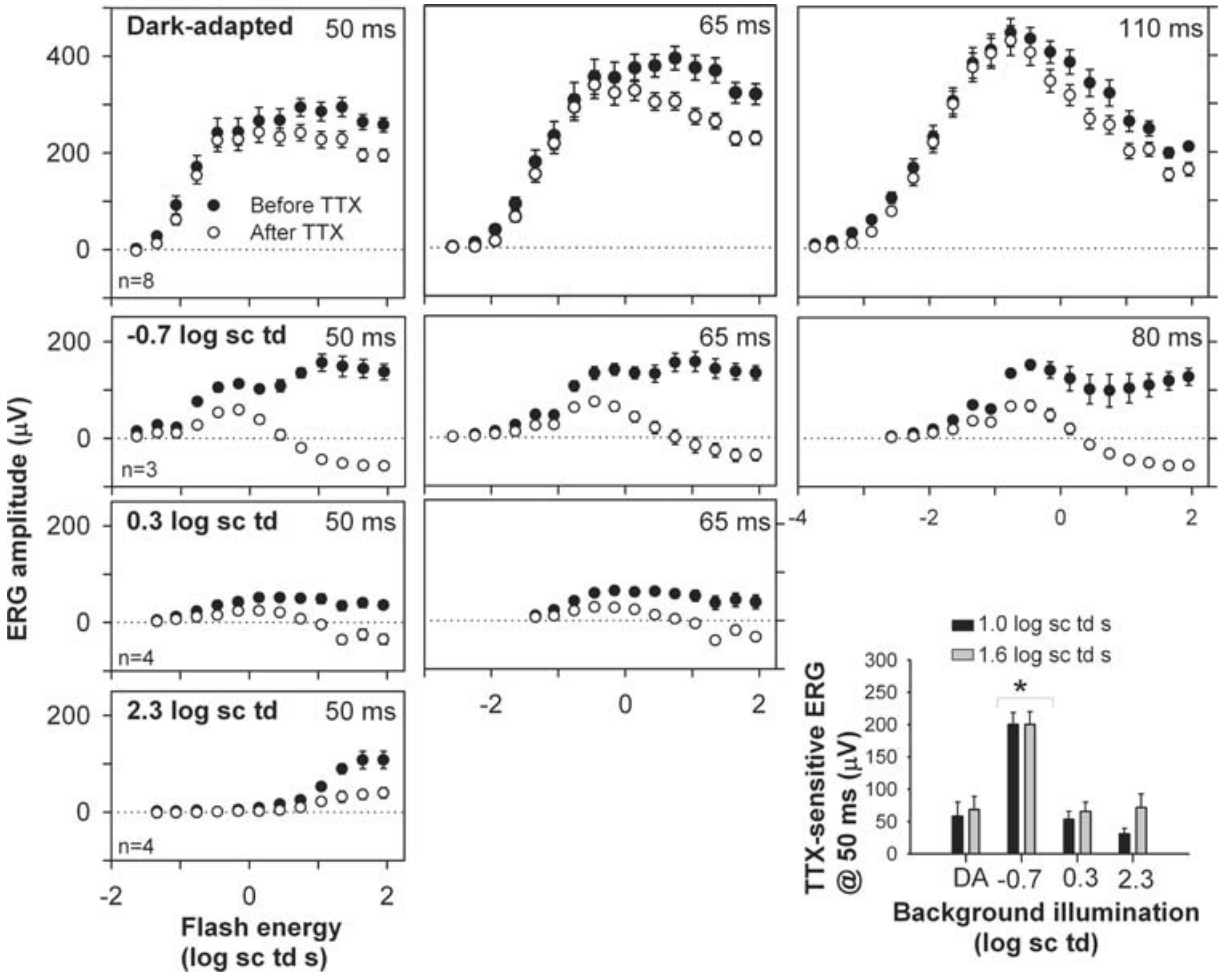

Figure 4. Stimulus–response relationship before and after TTX
ERG amplitudes measured at b-wave peak times under different stimulus conditions (group mean ± S.E.M.) plotted as a function of stimulus energy. Background illumination increased from top to bottom row. •, mean amplitudes before and ○, amplitudes after intravitreal TTX injection. Peak times increased from right to left. The bar hisotogram (bottom right) plots TTX-sensitive b-wave amplitudes measured at 50 ms (before TTX minus after TTX) as a function of background illumination for two stimulus energies: 1 log sc td s (black bars) and 1.6 log sc td s (grey bars). * TTX-sensitive amplitudes significantly different from the others (Tukey–Kramer *post hoc* test, $P < 0.05$).

in the rat (Xu *et al.* 2003; Bui & Fortune, 2004) than those after 1400 ms and longer time intervals when rod responses were recovering.

The time of cone signal recovery was determined for the range of stimulus energies used in this study where cone-driven responses were present (1.0–1.9 log sc td s). Figure 6 shows normalized b-wave amplitudes measured at a time to peak of 50 ms for test flashes of 1.3 log sc td s for four different background conditions. Results were similar for all flash energies when responses were normalized to the highest b-wave amplitude obtained for that energy for each background condition. Under dark-adapted conditions (left column in Fig. 6), the b-wave showed a two-stage recovery function. It was assumed that the first limb represented the recovery of cone signals arising from the cone to cone bipolar cell circuit, whereas the second limb represented recovery of rod signals. The time after extinguishing the conditioning flash for the cone-driven b-wave to reach a criterion saturation level, corroborated by the time for saturation of the small cone a-wave (bottom row of Fig. 6), was taken as the time for full recovery of the cone-driven response.

An exponential equation provided a good fit to the rise of the b-wave amplitudes up to the first asymptote ($R^2 > 95\%$). The equation used was:

$$\text{b-wave amplitude} = a + b(e^{-t/\tau})$$

where a represents the amplitude of the b-wave at the transient background, b is the b-wave V_{max}, τ is the time constant for b-wave recovery, and t is the time after conditioning flash. Curve fitting was carried out using the Marquardt–Levenberg algorithm in SigmaPlot 8 to find reasonable parameter values that minimized an equally

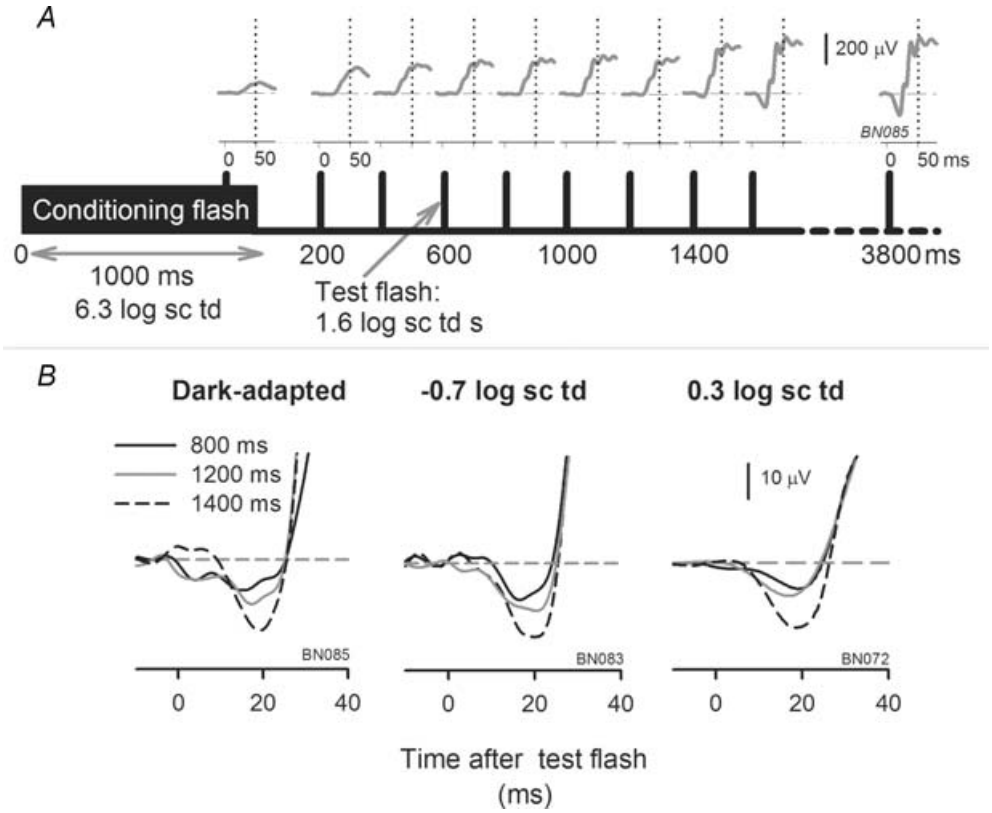

Figure 5. Protocol to isolate the cone-driven portion of the ERG
A, schematic diagram showing the protocol for determining the interstimulus interval for isolating cone-driven responses using a paired-flash protocol. A high energy conditioning flash (6.3 log sc td, 1000 ms duration), for any background (dark-adapted condition in this example, subject BN085) was used to suppress rods fully and cones partially. Test flashes (1.6 log sc td s) presented at incrementing intervals after the conditioning flash were used to follow recovery of the ERG. ERGs recorded in response to test flashes are shown above the time markers. The illustrated response was the difference of the ERG response to conditioning flash + test flash and the conditioning flash. The vertical dotted lines at 50 ms after the test flash show the cone ERG b-wave time to peak. The cone b-waves had almost fully recovered (93%) by 800 ms after offset of the conditioning flash. The ERG grew in size for later times as the rods recovered. *B*, the practically full recovery of the cone-driven a-wave at 800 ms, and the beginning of the recovery of the mixed rod + cone-driven a-waves at 1200 and 1400 ms after offset of the conditioning flash are illustrated on an expanded time scale.

weighted sum of squared differences between the data and the equation. A time constant (τ) of ~303 ms was derived from this equation for the dark-adapted, lower mesopic and photopic curves (see figure legend for details). For the higher mesopic background of 0.3 log sc td the same time constant produced a reasonable fit ($R^2 > 90\%$). This fit was imposed on the rising limb of the curve, because there was no clear asymptotic value for the curve. The fitted curves predicted that for a delay of ~800 ms after offset of the conditioning flash, the cone-driven b-wave had recovered to within ~93% of its full amplitude. This recovery time is similar to that found for mouse ERG (Lyubarsky *et al.* 1999), and is much longer than the 300 ms cone signal recovery time for humans and monkeys (e.g. Paupoo *et al.* 2000; Robson *et al.* 2003). The small cone-driven a-wave recovered with about the same time constant found for the b-wave. The a-wave was not present under photopic conditions for the stimulus energies used in this experiment. After the cone a-wave amplitude saturated, the initially nearly linear growth of the a-wave with time, in the bottom row of Fig. 6, shows the recovery of rod-driven signals.

As an additional confirmation that the cone-isolation protocol yielded a veridical estimate of cone-driven responses, ERGs measured on a steady rod-saturating background of 2.3 log sc td were compared to ERGs measured 800 ms after a cone-isolating conditioning flash on that background. The photopic ERGs produced by the standard protocol (black traces) and the cone-isolation protocol (grey traces) on the same eye of an animal are shown in Fig. 7*A*, and they are clearly similar. The inset to Fig. 7*A* shows averaged waveforms from four animals in response to a high energy flash (1.9 log sc td s) using the standard protocol and the cone-isolation protocol in the same eyes, plotted to show the similarity of the full time course of the responses. The b-wave peaking at 50 ms, and the PhNR following the b-wave, with a trough at 200 ms can be seen to be similar under the two conditions (paired *t* test evaluated at 50 ms and 200 ms for $P < 0.05$).

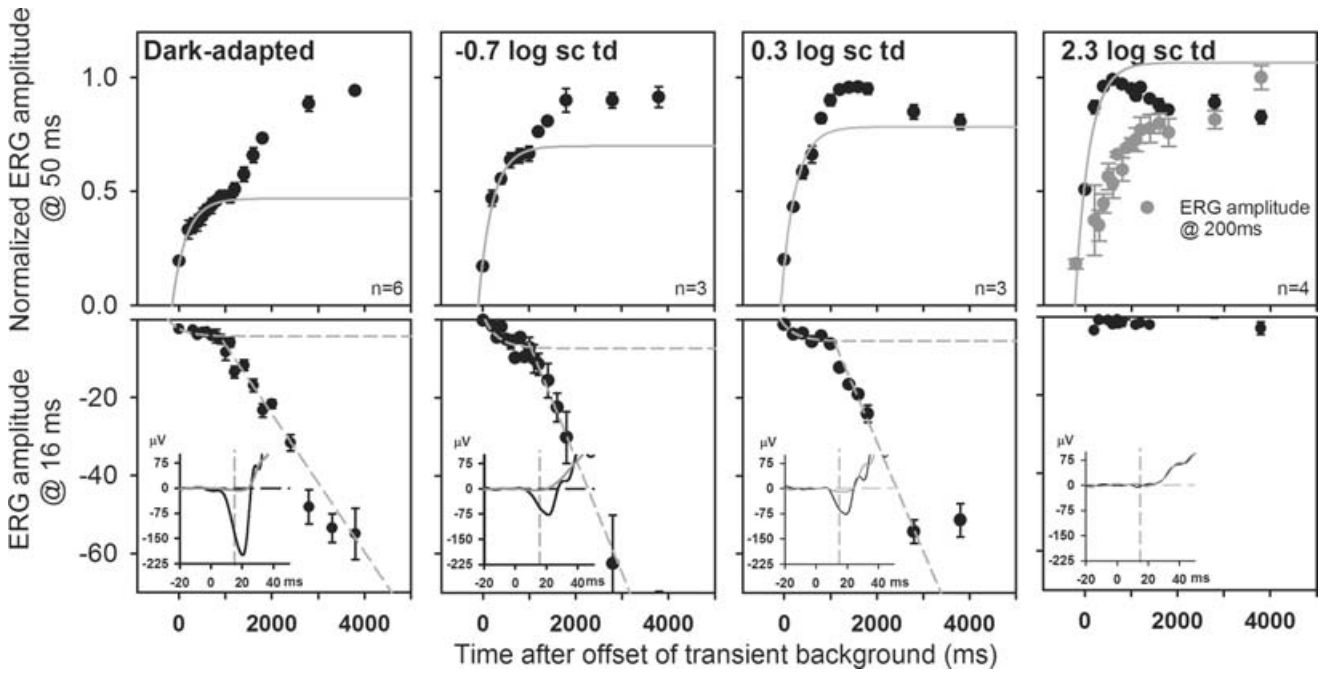

Figure 6. Deriving the interstimulus interval for isolating cone responses
Upper row: the growth of normalized peak (50 ms) b-wave amplitude for a 1.3 log sc td s test flash (mean ± S.E.M.) after offset of the transient background (6.3 log sc td) showed two limbs at all backgrounds except 2.3 log sc td, when rods were suppressed. The first limb, all points (cone-driven) were fitted for all backgrounds with an exponential with a time constant of ~303 ms ($R^2 > 95\%$ for dark-adapted and backgrounds of −0.7 and 2.3 log sc td). For the background of 0.3 log sc td there was no clear asymptotic value, the first 4 data points and a time constant of 303 ms were used to fit the exponential curve ($R^2 > 90\%$). The cone-driven b-wave had recovered to ~93% of its V_{max} 800 ms after offset of the transient background. Lower row: the a-waves (1.6 log sc td s test flash) were measured at 16 ms after the flash on the leading edge of the small cone-driven a-wave (see inset, grey traces, cone-driven; black traces, full flash). The growth of the small cone-driven a-wave was fitted with an exponential function with the same time constant of ~303 ms ($R^2 > 80\%$). The second limb of a-wave growth showed an initial linear rise, which, when regressed ($R^2 > 95\%$) to the baseline, indicated that the cone-driven contribution to the a-wave was negligible at 800 ms after the conditioning flash.

Figure 7*B* shows the stimulus–response curves for cone-isolated ERGs measured at a b-wave peak time of 50 ms for the four background conditions studied. The amplitude was slightly reduced by the mesopic backgrounds relative to dark-adapted conditions, but the reduction was not statistically significant (*t* test; $P < 0.05$). However, when the 2.3 log sc td background was present, the maximum amplitude was significantly lower than that under dark-adapted conditions, indicating an adapting effect of the background on the cone-driven responses.

Effects of TTX on the cone-isolated ERG

Typical cone-isolated ERGs before and after TTX injection are illustrated in Fig. 8. TTX reduced the b-wave amplitude at every background level. Unlike the findings for the mixed rod–cone ERG, reductions were largest under dark-adapted conditions, and decreased with increasing background level, although for photopic conditions, effects were usually greater than shown for the response to a 1.9 log sc td s stimulus in this figure. At mesopic levels, the b-wave after TTX always remained above baseline rather than moving below as it had done when rod signals were present (e.g. Figs 1, 2 and 4). The b-wave also appeared to be less transient after TTX for the dark-adapted and mesopic conditions. This observation was not analysed further in the present report.

Average cone-driven b-wave amplitudes, measured before and after TTX, are plotted in Fig. 9*A*. The plots show attenuation of the b-wave under all background conditions as seen in Fig. 8. For the purpose of uniformity we measured amplitudes at 50 ms, although the dark-adapted cone-isolated b-waves peaked closer to 65 ms. The data were plotted on log–log axes in Fig. 9*A* to more easily view the reduction both in the maximum amplitude (V_{max}) and responsivity (K) that occurred after TTX. The data were fitted with hyperbolic saturation functions. The equation used was:

$$V = \frac{V_{max}\,E}{V_{max}/K + E}$$

where V represents ERG amplitude at 50 ms, V_{max} is the maximum saturated ERG amplitude at 50 ms, K is the responsivity (V_{max}/E_0), E is flash energy, and E_0 is flash energy at $V_{max}/2$.

The parameters for these fits are presented in Table 4. They show a decrease in both V_{max} and responsivity (i.e. gain) due to TTX that is greatest under dark-adapted conditions, and least under photopic conditions. Implications of these findings with respect to the role of Na_v channels in the outer retina will be addressed in the Discussion.

Rod *versus* cone contributions to the b-wave

The stimulus–response functions for mixed rod–cone responses of animals used in cone-isolation experiments are shown in Fig. 9*B*. For each background, the results are shown for control ERGs and ERGs after TTX. For comparison, the control cone-isolated responses in Fig. 9*A* are included in the graphs. The stimulus energy that produced responses of 10 μV for the cone-isolated

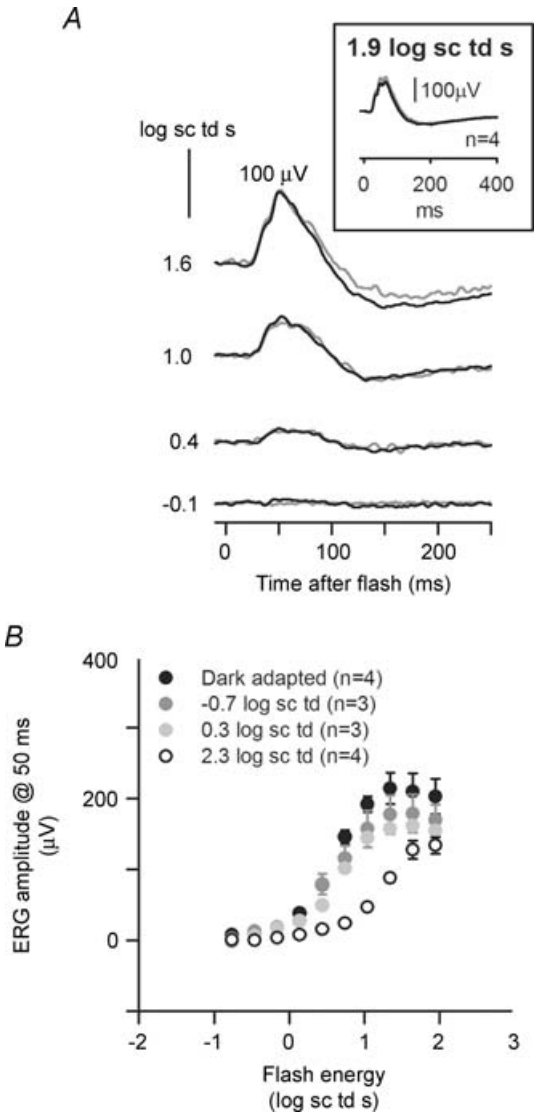

Figure 7. Effect of cone isolation under rod-suppressed (photopic) conditions (2.3 log sc td)
A, comparison of ERGs recorded in the presence of the steady photopic background (2.3 log sc td) using either the paired flash protocol to isolate cone signals (grey trace) or normal single flashes (black trace) for a single subject. The inset shows that the average ERG waveforms ($n = 4$) recorded for the same subjects using both protocols were similar. *B*, light adaptation of the cone-isolated energy response functions. Amplitudes (group mean ± S.E.M.) measured at 50 ms near the peak of the cone-driven b-wave as a function of stimulus energy for four different background conditions.

responses (calculated from the hyperbolic fits in panel *A*) was taken as a rough approximate 'threshold' for cone signals at each background level (except 2.3 log sc td s which was already producing photopic conditions). In the top three plots in Fig. 9*B*, a dashed vertical line marks the 'threshold' energy point on the *X*-axis.

Figure 9*B*, top plot, shows that for the dark-adapted condition, significant cone signals were isolated only after the first saturation of the mixed rod–cone b-wave (measured at 50 ms after the flash), indicating that before that first saturation the signals reflected responses mediated by rod bipolar cells. This conclusion is consistent with previous findings in rodents (Toda *et al.* 1999; Nixon *et al.* 2001). It is important to note that TTX did not affect the stimulus–response curve until past the first saturation when cones were active, suggesting that TTX affected circuits mediated by cone rather than rod bipolar cells.

When the −0.7 log sc td background was present (second panel in Fig. 9*B*) the leftmost three data points for the low-amplitude (nearly flat) (rod bipolar cell-driven) limb of the stimulus–response curve was also not significantly affected by TTX ($P > 0.05$). In contrast, TTX reduced the response to all higher stimulus energies. For the higher energies, when rod signals were involved, they were probably travelling in the second rod pathway, i.e. in a cone bipolar cell-mediated circuit, as is considered more fully in the Discussion. For the higher mesopic background of 0.3 log sc td, there was only one rising limb of the curve and TTX effects occurred mainly after the cones became active.

To determine the background conditions for which the cone-isolated *versus* mixed rod–cone ERGs were maximally sensitive to TTX, responses after TTX were subtracted from those before TTX in the same eye. For each background, the amplitude of the response removed by TTX (measured at 50 ms), i.e. the TTX-sensitive response, grew with stimulus energy up to the energies where response curves saturated (data not shown). Figure 9*C* shows a comparison of TTX-sensitive responses to a stimulus of 1.0 log sc td s on the left, and 1.6 log sc td s on the right.

The TTX-sensitive cone-isolated b-waves (white bars) under dark-adapted conditions were significantly larger than the TTX-sensitive mixed rod–cone b-waves for both energies illustrated in Fig. 9*C* ($P < 0.05$). In contrast, for the lower mesopic background where the mixed rod–cone component was largest, the cone-isolated response was signficantly smaller than the mixed response ($P < 0.05$). For the higher mesopic level (0.3 log sc td), the cone-isolated responses were again significantly larger ($P < 0.05$), and for the photopic condition, both responses, being completely cone-driven, were of similar amplitude. Possible mechanisms for these adaptational effects are addressed in the next sections.

Identity of the retinal neurons contributing to the TTX-sensitive b-wave

The TTX-sensitive retinal mechanisms contributing to the ERG b-wave could be due to effects of TTX on Na_v channels

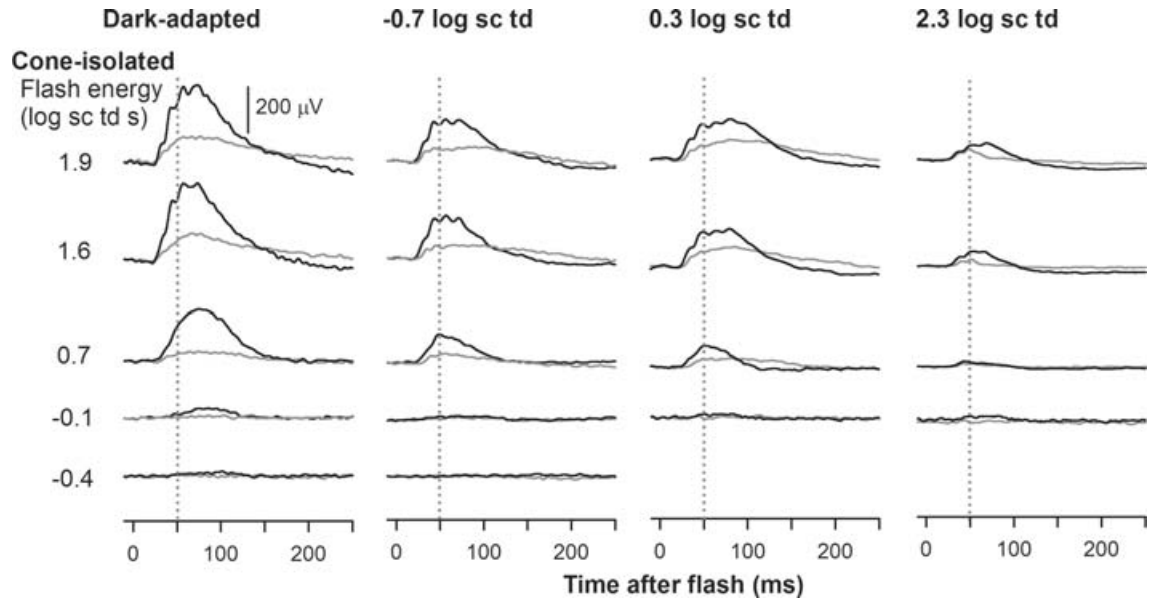

Figure 8. Effect of TTX on the cone-isolated ERG response for different background conditions
Black traces represent cone-isolated ERGs produced by the paired-flash protocol (ISI = 800 ms) before TTX and grey traces represent those after TTX for four different backgrounds in four representative subjects.

Table 4. Parameters of hyperbolic curve fits to cone-isolated b-wave amplitudes (50 ms) as a function of stimulus energy

Background illumination (log sc td)	V_{max} (μV)	± S.E.M.	E_o (Sc td s)	± S.E.M.	K (μV (sc td s)$^{-1}$)	± S.E.M.	R^2
Before TTX							
DA	236	15.0	4.3	1.1	54.8	14.1	0.96
−0.7	196	10.0	4.2	0.9	46.7	9.9	0.96
0.3	185	11.0	5.3	1.0	35.0	7.1	0.96
2.3	178	13.0	27.4	6.5	6.8	1.8	0.97
After TTX							
DA	68.9	3.4	5.2	1.0	13.1	2.5	0.97
−0.7	57.3	4.5	3.6	1.2	16.1	5.2	0.93
0.3	66.9	4.4	4.9	1.2	13.8	3.6	0.93
2.3	68.5	6.8	17.5	4.9	3.7	1.1	0.94

of retinal ganglion cells or more distal retinal neurons with functional channels. To determine if retinal ganglion cells were involved, the optic nerve was transected (ONTx) and ERGs were recorded 3–6 weeks later when ganglion cells had degenerated (see below). This allowed us to observe the effects of ganglion cell loss on the ERG directly, as well as the effects of TTX on ERGs in eyes lacking ganglion cells. As noted in the Methods, a perilacrimal route was chosen for the ONTx surgery to avoid injury to the eyeball or its blood supply. This protocol is different from the one used in a previous similar study in Brown Norway rat by Bui & Fortune (2004) and one by Li *et al.* (2005) that examined only the photopic ERG, but, as shown below, it was effective in eliminating ganglion cells for all time points used.

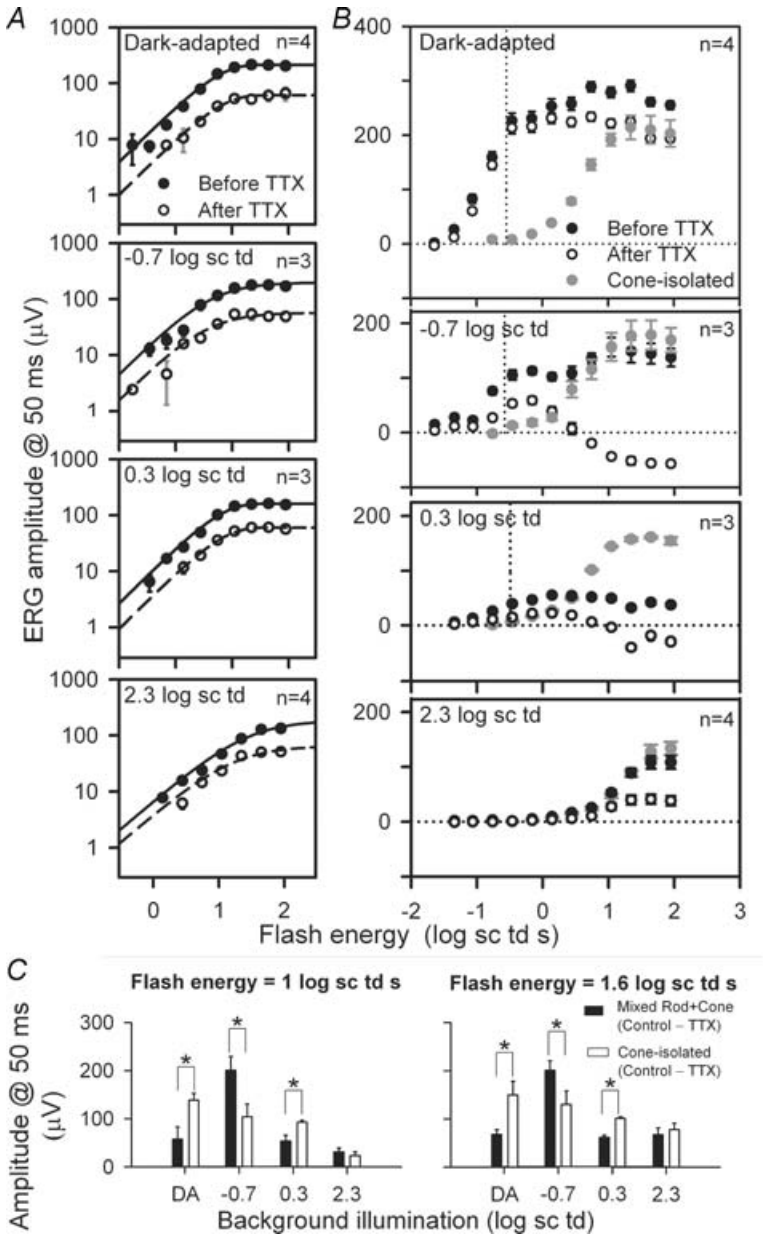

Figure 9. Effect of TTX on rod-, mixed rod + cone-, and cone-driven ERGs
A, amplitudes of the cone-isolated ERGs (group mean ± S.E.M.) plotted as a function of stimulus energy before (black circles) and after (white circles) TTX injection for the dark-adapted condition and backgrounds of −0.7, 0.3 and 2.3 log sc td (top to bottom). Responses were measured at 50 ms after the flash in all cases. The continuous black and dashed black curves represent hyperbolic saturation functions fitted to the ERG amplitudes before and after TTX, respectively. *B*, ERG amplitudes of mixed rod–cone ERGs for the same eyes as in *A* and a subset of the data in Fig. 4 (group mean ± S.E.M.) plotted as a function of stimulus energy before (black circles) and after (white circles) TTX injection, for the dark-adapted condition and backgrounds of −0.7, 0.3 and 2.3 log sc td (top to bottom). Grey circles represent the cone-isolated ERG amplitudes for the same animals before TTX. All responses were measured at 50 ms after the flash. The vertical dotted line represents flash energy that produces 10 μV of the maximum cone-isolated ERG amplitude for each background, except the photopic one. *C*, TTX-sensitive (before TTX – after TTX) ERG amplitudes, measured at 50 ms (group mean ± S.E.M.) for the mixed rod + cone ERG (black bars) compared to those for the cone-isolated ERG (white bars), for flash energies of 1 log sc td (left) and 1.6 log sc td (right). * TTX-sensitive amplitudes significantly different from the others (*t* test; $P < 0.05$).

Optic nerve transection caused a selective loss of retinal ganglion cells

To evaluate the ability of ONTx to eliminate retinal ganglion cells and their dendrites and axons selectively, we examined labelling for several known ganglion cell markers in frozen sections of the retinas from eyes receiving ONTx and their fellow untreated control eyes. To compare retinal anatomy and physiology, these studies were carried out on eyes collected from animals 3–6 weeks after ONTx was performed, after ERG recordings were completed. Sections that passed through the central retina including the optic nerve head and optic nerve were specifically selected for these studies.

ONTx virtually eliminated all ganglion cells and their processes after 3–6 weeks (Fig. 10; neurofilament 200 kDa: ganglion and horizontal cell axons; MAP-1, ganglion cell dendrites, cell bodies and axons; and Brn-3a, ganglion

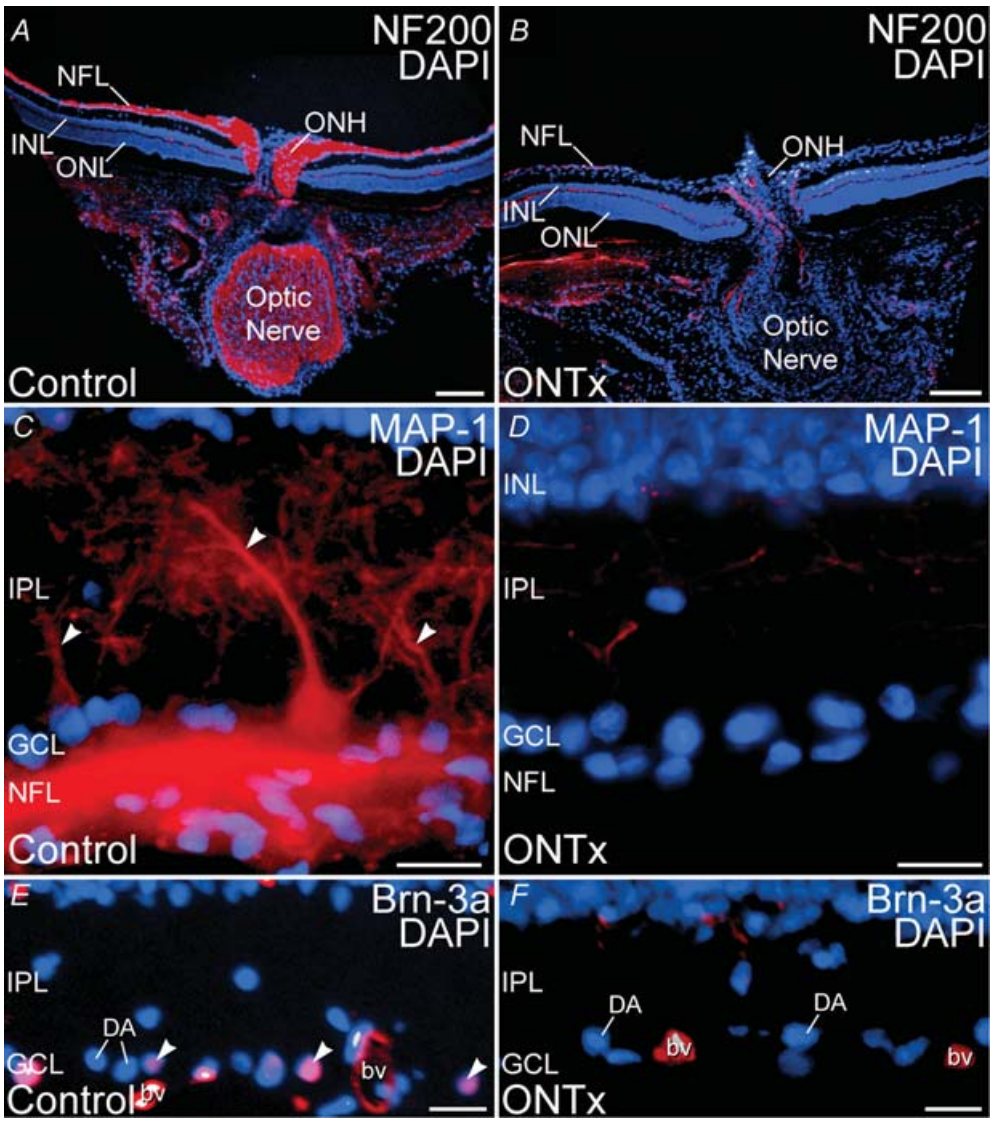

Figure 10. Optic nerve transection (ONTx) ablated retinal ganglion cells 3–6 weeks after surgery
Immunolabelling for ganglion cell-specific markers is eliminated by ONTx. *A* and *B*, double labelling for neurofilament 200 kDa (NF200, red) and the nuclear dye DAPI (blue) in control retina (*A*) and retina 4 weeks after ONTx (*B*). *C* and *D*, double labelling for MAP-1 (red) and DAPI (blue) in control retina (*C*) and retina 6 weeks after ONTx (*D*). Large MAP-1-positive ganglion cell dendrites (arrowheads) are absent in the IPL after ONTx. *E* and *F*, double labelling for Brn-3a (red) and DAPI (blue) in the control retina (*E*) and retina 6 weeks after ONTx (*F*). Ganglion cell nuclei showing double labelling (arrowheads) are present in the control retina, but absent from ONTx retina. Displaced amacrine cells (DA) in the ganglion cell layer (GCL), however, persist in ONTx retina. Labelling in blood vessels (bv) is non-specific. ONL, outer nuclear layer; INL, inner nuclear layer; IPL, inner plexiform layer; NFL, nerve fibre layer. Scale bars: 200 μm for *A* and *B*; 20 μm for *C*–*F*.

cell nuclei). The elimination of ganglion cells and their processes by ONTx was highly selective. Although ONTx ablated ganglion cells, labelling by the nuclear dye DAPI (see Fig. 10) and calretinin, a marker for displaced starburst amacrine cells in the ganglion cell layer (GCL) (not shown), indicated that displaced amacrine cells persisted in the GCL. DAPI labelling also showed that ONTx did not cause disruption of cells in the ONL or INL (Fig. 10). Immunolabelling for specific markers for horizontal cells (calbindin, neurofilament 200 kDa), amacrine cells (calbindin, calretinin, ChAT), rod bipolar cells (PKCα subunit), and photoreceptor and bipolar cell ribbon synapses (VGluT1; Johnson *et al.* 2003; Sherry *et al.* 2003*a*) were also not affected by ONTx (data not shown). Labelling for glial fibrillary acidic protein (GFAP), an astrocyte marker (Dixon & Eng, 1980), was present in the astrocytes of both control and ONTx retinas. However, Müller cells showed GFAP labelling only in the ONTx retina (data not shown), as reported previously for rat retinas with optic nerve damage (Bignami & Dahl, 1979). Thus, the cell loss produced by ONTx was selective for ganglion cells.

ONTx did not reduce the amplitude of the b-wave

Figure 11, left column, shows ERG recordings from an ONTx eye (grey lines), and the control fellow eye (black lines), 4 weeks after ON transection, when ganglion cells would have degenerated. ONTx, as previously described (Bui & Fortune, 2004), reduced the amplitude of the pSTR, and the later part of the nSTR. The middle column of Fig. 11 shows typical findings for a high energy flash (1.6 log sc td): minimal effects on b-waves for all backgrounds, a slight reduction of the slow negative wave after the b-wave in mesopic conditions, and no effect on the PhNR under photopic conditions. These findings were similar for all animals tested between 3 and 6 weeks after ONTx. Figure 12, left column, shows plots of the average stimulus–response curves measured at 50 ms after the flash for the ONTx eyes (grey circles) and control fellow eyes (black circles). As noted above, the photopic ERG results in this study are different from those of Bui & Fortune (2004) where a decrease in the photopic b-wave amplitude was reported. However, the ganglion cell-related responses (pSTR and nSTR) were affected similarly in the two studies, and both studies documented with histology the loss of ganglion cells. Li *et al.* (2005) studied photopic ERGs in rats after ONTx and ganglion cell degeneration, and also did not see a change in photopic b-wave. However, our results differed from Li *et al.* (2005) who observed the PhNR to be reduced, whereas we did not. Possible reasons for the preservation of the photopic b-wave and PhNR in the present study will be addressed in the Discussion.

The right column of Fig. 11 compares ERGs from the ONTx eye, already illustrated in the middle column (grey line), with ERGs from the same eye after TTX injection (dotted traces). The effects of TTX in the ONTx eye were similar to the effects of TTX on the ERG of intact retinas described earlier in this paper. This observation was made previously for dark-adapted ERGs only (Bui & Fortune, 2004). Although photopic ERGs of ONTx eyes were not tested with TTX, results for other backgrounds and all other studies in normal eyes predict that they would have been reduced.

The right column of Fig. 12 compares the ERGs in the ONTx eyes (grey circles) with the ERGs from the same eyes after TTX injection (ONTx + TTX, white circles). Effects of TTX in ONTx eyes were similar to effects in intact eyes (compare with plots in Figs 4 and 9*B*), indicating that TTX effects on the ERG b-wave amplitude were mediated by neurons distal to the ganglion cells.

Effects of TTX on the ERG after blocking inner retinal activity

The experiments in the previous section showed that retinal ganglion cells were not involved in mediating the TTX effects on the b-wave observed in the present study. The experiments in this section were done to try to separate the effects of TTX on amacrine cells from those occurring more distally, directly on the bipolar cells, for example.

The approach was to use intravitreal injections of agents that would suppress inner retinal responses. Ionotropic glutamate receptor blockers, such as CNQX, will block AMPA/KA receptors (e.g. Bleakman & Lodge, 1998) that are present on dendrites of inner retinal neurons (as well as on OFF bipolar and horizontal cells). CNQX (200 μM) was shown to be useful in this regard in a previous study from this laboratory (Mojumder *et al.* 2007) in which effects of TTX were observed on the dark-adapted cone-isolated ERG. However, CNQX has been found to reduce the amplitude of the rod-driven b-wave (Bui & Fortune, 2004), and this reduction also occurs with other ionotropic glutamate receptor blockers: PDA (*cis*-2,3-piperidine-dicarboxylic acid, 3–5 mM; Bui & Fortune, 2004; DK Mojumder & LJ Frishman, unpublished observations), and DNQX (6,7-dinitroquinoxaline-2,3-dione, 200 μM; authors' unpublished observations) limiting their value for the present study of mixed rod–cone ERGs under dark-adapted and mesopic conditions. Examples of the effect of CNQX on the dark-adapted and cone-isolated ERG from data included in Mojumder *et al.* (2007) are shown in Fig. 13*C*. For the cone-isolated ERG, as previously reported, TTX had its full effect in the presence of CNQX.

In a further attempt to suppress inner retinal activity before injecting TTX, the glutamate agonist NMDA was used. Functional NMDA receptors are found mainly on ganglion cells and on some amacrine cells rather than on more distal neurons in the retina (Massey &

Miller, 1990; Cohen & Miller, 1994; Massey & McGuire, 1998, for review). NMDA is thought to depolarize inner retina neurons, making them unresponsive to light (e.g. Robson & Frishman, 1995). NMDA might also induce, via depolarization of amacrine cells, release of the inhibitory neurotransmitter GABA, and similarly, glycine (Calaza *et al.* 2001), which could enhance any inner retinal response suppression caused by NMDA. Under dark-adapted conditions, NMDA has been shown to be effective in mammals in eliminating elements of the ERG that originate from the inner retina, the sensitive positive and negative STRs, thereby isolating what is likely to be the rod bipolar cell component of the ERG (Robson & Frishman, 1995; Naarendorp *et al.* 2001). Such an effect is illustrated for the dose that we used in Fig. 13*A*, and explained further in the figure legend. The effects of NMDA on light-adapted responses when cone circuits are active also will affect the inner retinal contributions of

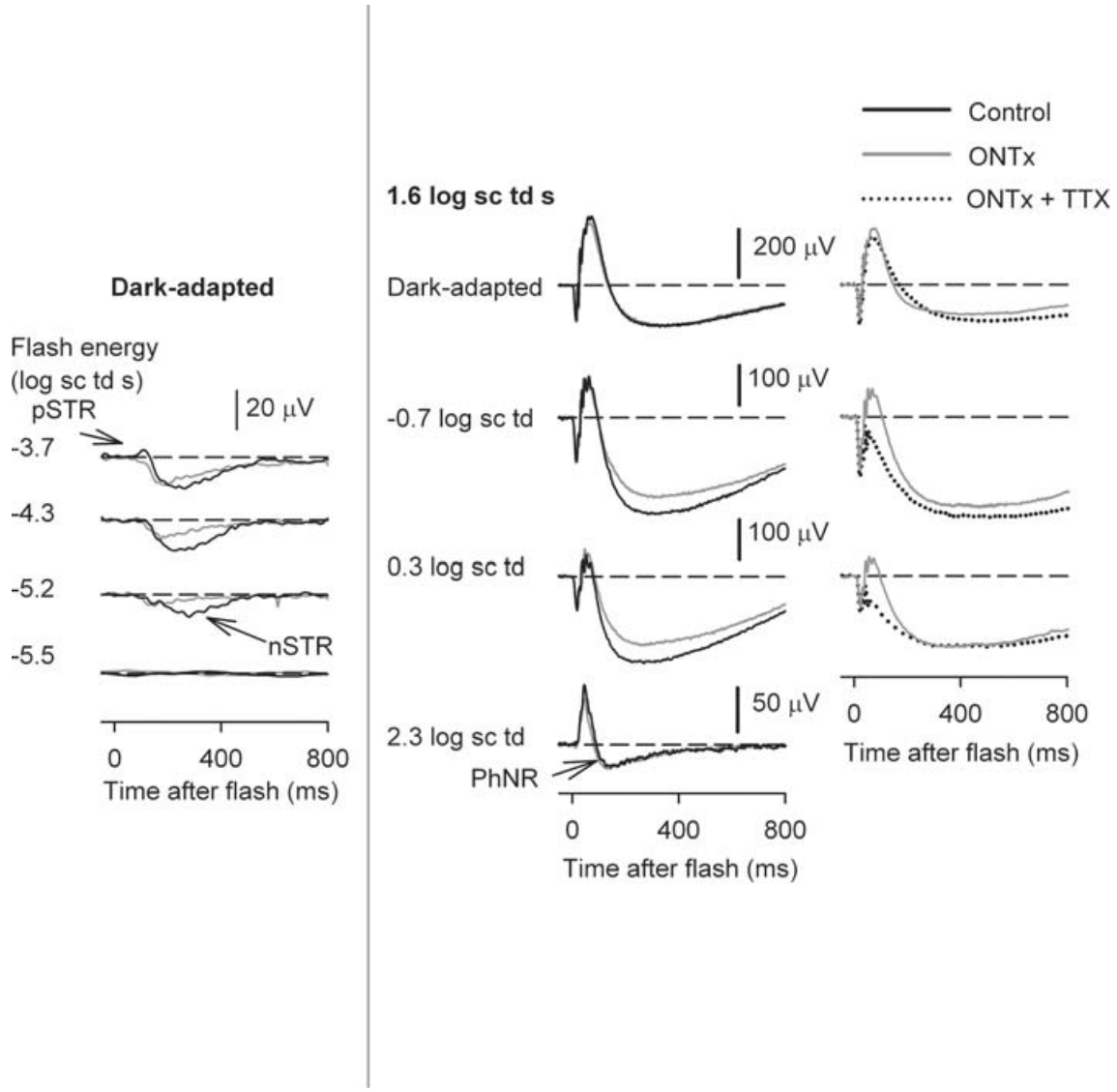

Figure 11. ERGs recorded after ONTx and ONTx + TTX
Left column: ERG responses to low energy flashes (from bottom to top: –5.5 to –3.7 log sc td s) to show the effects of ONTx (grey lines) on the negative scotopic threshold response (nSTR) and the positive STR. The responses are compared to those of the fellow control eye (black line) recorded in the same experimental session. Middle column: ERG responses to a high energy flash (1.6 log sc td s) under dark-adapted conditions, and in the presence of steady background illumination (increasing from top to bottom), for the ONTx eye and the control eye. Right column: ERG responses to a high energy flash (1.6 log sc td s) for incrementing background illumination (top to bottom), for the same ONTx result (grey line) shown in the middle column (grey line), and following TTX injection in the same eye (dotted trace). All ERGs in this figure were recorded 4 weeks after ONTx.

photopic ERGs (e.g. Rangaswamy *et al.* 2003; Sharma *et al.* 2005), although not completely (see below). Intravitreal injection of TTX following NMDA, was used to look for the remaining effects of TTX on the b-wave.

Figure 13*B* shows typical effects of NMDA on the ERG elicited by a high energy flash (1.6 log sc td, grey trace), and TTX after NMDA (dotted trace) under different background conditions. The dark-adapted cone-isolated ERGs were chosen for illustration because amplitudes were larger than those under photopic conditions (see Fig. 7*B*). The figure shows that across background conditions, NMDA hardly affected the responses to this stimulus, except for a small reduction in the cone-isolated b-wave. Small effects on photopic ERG b-waves have been observed previously (Bui & Fortune, 2004). The small changes in Fig. 7*B* in a-waves and negative waves after the b-wave were not consistent across eyes. OPs that are believed to originate mainly from amacrine cells (see Wachtmeister, 1998, for review), remained after NMDA injection as reported previously (Bui & Fortune, 2004), raising the possibility of incomplete inner retinal blockade (or more bipolar cell involvement in generation of OPs than generally appreciated). Addition of TTX to the eye already injected with NMDA (dotted line) reduced the b-wave under all background conditions, although the effect of TTX looked smaller for the mesopic backgrounds than effects of TTX alone (Figs 1 and 2). The next figure quantifies the results for the eyes injected with NMDA and NMDA + TTX.

Figure 14 compares results of TTX injections after NMDA with results when TTX was injected in control eyes (from Fig. 4, bottom plot in the right-hand column). Because control b-wave amplitudes tended to be more similar for given sets of experiments than across all experiments, the TTX-sensitive b-wave amplitude was normalized to the control b-wave amplitude for the same experiment ((Control – TTX)/Control; black bars) and the NMDA + TTX-sensitive b-wave amplitude normalized to the undrugged control b-wave amplitude

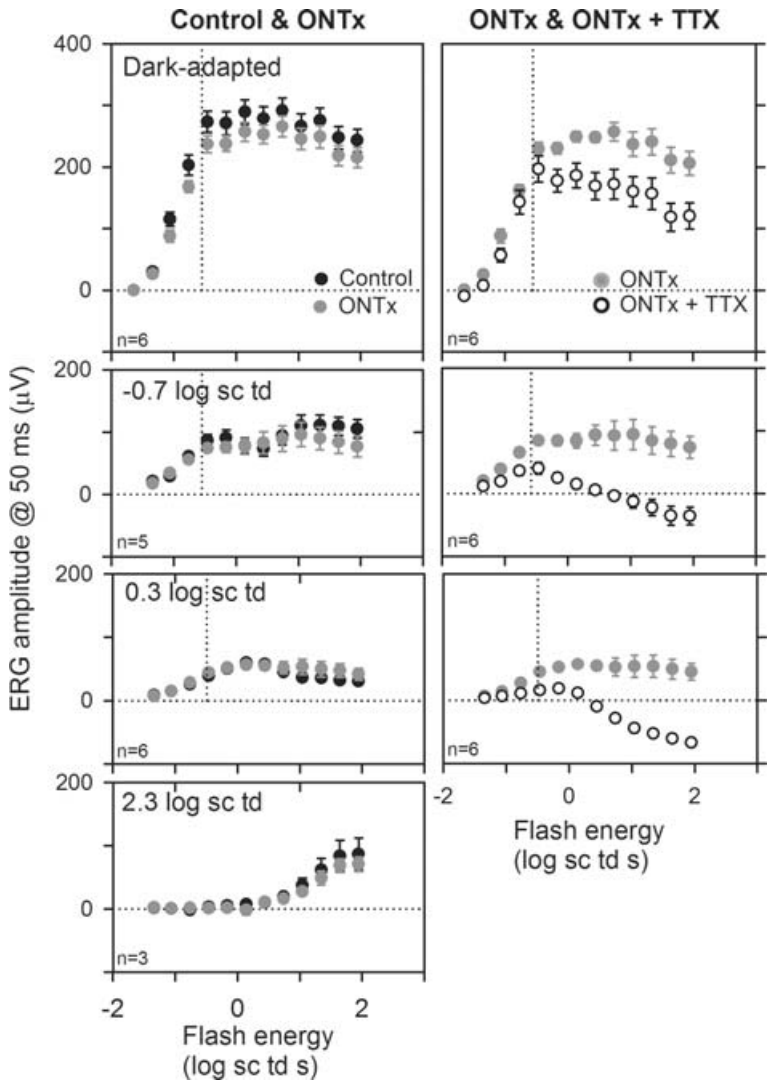

Figure 12. Effects of ONTx and ONTx + TTX on ERG amplitudes
Left column: ERG amplitudes (measured at 50 ms after the brief flash) (group mean ± S.E.M.) plotted as a function of stimulus energy for the ONTx eye (grey circles) and the fellow control eye (black circles) for the dark-adapted condition and backgrounds of −0.7, 0.3 and 2.3 log sc td (top to bottom). Right column: ERG amplitudes (group mean ± S.E.M.) plotted as a function of stimulus energy for the ONTx eye (grey circles) and after ONTx + TTX (white circles). The vertical dotted line represents the flash energy that produces 10 μV of the maximum cone-isolated ERG amplitude measured at 50 ms for each condition of background illumination.

in that experiment (Control – (NMDA + TTX)/Control; grey bars). The comparison was done for responses to flash energies used for comparisions in other figures: 1.0 and 1.6 log sc td s. Both plots in Fig. 14 show that for dark-adapted and cone-isolated conditions, results after TTX alone and NMDA + TTX were not significantly different (t test, for $P < 0.05$), indicating a locus for the TTX effects distal to amacrine and ganglion cells whose activity would have been suppressed by NMDA. However, for the background of −0.7 log sc td for both stimuli, and also the 0.3 log sc td background for the stronger stimulus, TTX-sensitive b-waves represented a smaller proportion of the control response in eyes injected with NMDA than in eyes injected only with TTX (t test; $P < 0.05$). The finding that NMDA reduced, but did not eliminate the TTX effects found under mesopic conditions suggests that the large mesopic effects involved NMDA-sensitive inner retinal neurons, in addition to the more distal elements, i.e. cone bipolar cells. The inner retinal cells involved were likely to be amacrine cells, as loss of ganglion cells due to ONTx had no effect on TTX-sensitivity of the b-wave. For each background, the post-TTX results after NMDA were also normalized to the result after NMDA alone (white bars), to show that the results were not just due to changes already present after NMDA. This was particularly important for the cone-isolated result for the 1.6 log sc td flash where NMDA caused a small, but not significant, reduction of b-wave amplitude (paired t test; $P > 0.05$). Results illustrated by black and white bars were not significantly different for this, or any background condition (paired t test; $P > 0.05$).

As noted above, in a previous study of the cone-isolated response, we reported that CNQX alone does not affect the b-wave amplitude, and that TTX retains its full effect in the

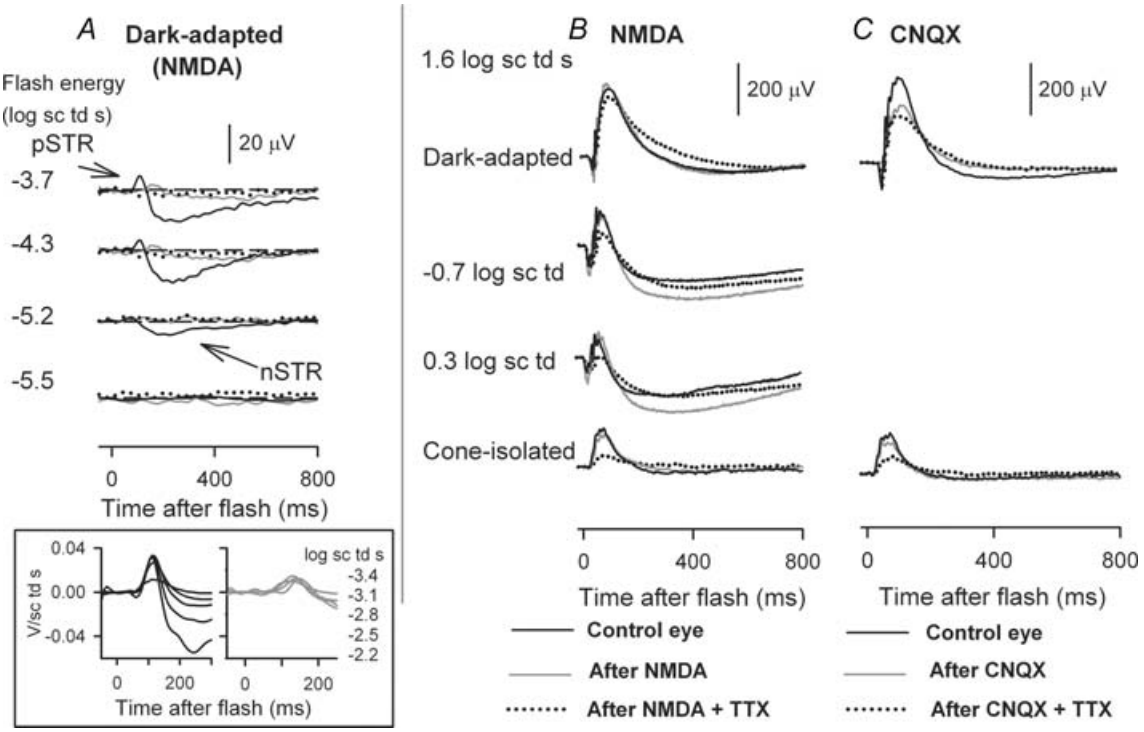

Figure 13. Effects of TTX on the ERG following suppression of inner retinal activity
Black traces indicate control responses before injection of pharmacological agents, grey traces, after NMDA, and dotted black traces after TTX and NMDA (NMDA + TTX) for the same eye. *A*, ERG responses to low energy flashes (from bottom to top: –5.5 to –3.7 log sc td s) to show the effects of NMDA (grey lines) and NMDA + TTX (dotted lines) on the negative scotopic threshold response (nSTR) and the positive STR (pSTR). The inset at the bottom shows energy-scaled responses for the indicated flash energies. Scaling each response by dividing by the stimulus energy used to produce it showed that responses after NMDA (right plot) were superimposed, and less sensitive than the positive- and negative-going response before NMDA (left). These findings are consistent with isolation of a single component (PII, the rod bipolar cell component) after NMDA. In the control records (left) both positive and negative STRs were present, as well as a less sensitive response to the strongest stimulus (–2.2 log sc td) that looked similar to the responses after NMDA. For more details of this type of analysis see Robson & Frishman (1995) and Robson *et al.* (2004). *B*, top to bottom, ERG responses to a high energy flash (1.6 log sc td s) for dark-adapted conditions, mesopic conditions, and under dark-adapted conditions when cone responses were isolated. *A*, effect of CNQX and TTX after CNQX on the dark- and cone-isolated ERG response to the same high energy flash (1.6 log sc td s). Data traces analysed in Mojumder *et al.* (2007), but not illustrated.

presence of CNQX (Mojumder *et al.* 2007). Data from that study are included for comparision in Fig. 14 at the far right of each plot where normalized TTX-sensitive responses after CNQX ((Control – CNQX + TTX)/Control) are shown. The CNQX result supports and extends the results after NMDA for cone-isolated conditions, suggesting that these effects of TTX were directly on Na_v channels in ON cone bipolar cells. Effects on all other elements but cone photoreceptors should have been eliminated by the CNQX, and contributions from Na_v channels on cones were unlikely to be involved, as addressed in the Discussion.

As noted above, responses in Fig. 14 were normalized to controls in the same experiment due to variation across experiments in b-wave amplitudes. A benefit of this normalization is that it shows that effects of TTX were proportionally greater for the cone-isolated b-wave than for the mixed rod–cone b-wave, and proportionally greater for mixed rod–cone ERGs under the two mesopic conditions than either scotopic or cone-isolated conditions (one-way ANOVA, $P = 0.0006$; Fisher's least squares difference *post hoc* test 95% confidence interval).

Discussion

This study examined the effects of blocking Na_v channels with TTX on the rat ERG. In addition to the expected attenuation of potentials known to originate from spiking neurons in the inner retina in rat, i.e. the n- and pSTR, and probably the photopic negative response, there was also a substantial reduction of the b-wave, an ERG wave that is generated mainly by bipolar cells. The reduction of the b-wave was present not only under photopic conditions, as previously observed (Bui & Fortune, 2004), but also under dark-adapted conditions when high energy flashes were used, and under mesopic conditions, for a range of flash energies. In fact, in this study, the effects of TTX were found to be greatest under mesopic conditions. Further investigations revealed marked effects of TTX on cone-isolated ERG that were largest under dark-adapated conditions. The effects on cone-driven responses were probably due to direct effects on Na_v channels on cone bipolar cells. Blockade of Na_v channels in amacrine cells might have been responsible for the large effects of TTX on the ERG seen under mesopic conditions.

Effects of ONTx and subsequent ganglion cell degeneration on the ERG: comparison with previous studies

The present study looked for inner retinal origins of the TTX effects on the ERG. In this context, a role for ganglion cells was examined following ONTx and subsequent loss of ganglion cells. Unlike previous findings (Bui & Fortune, 2004) in which a 25–30% reduction in the photopic b-wave

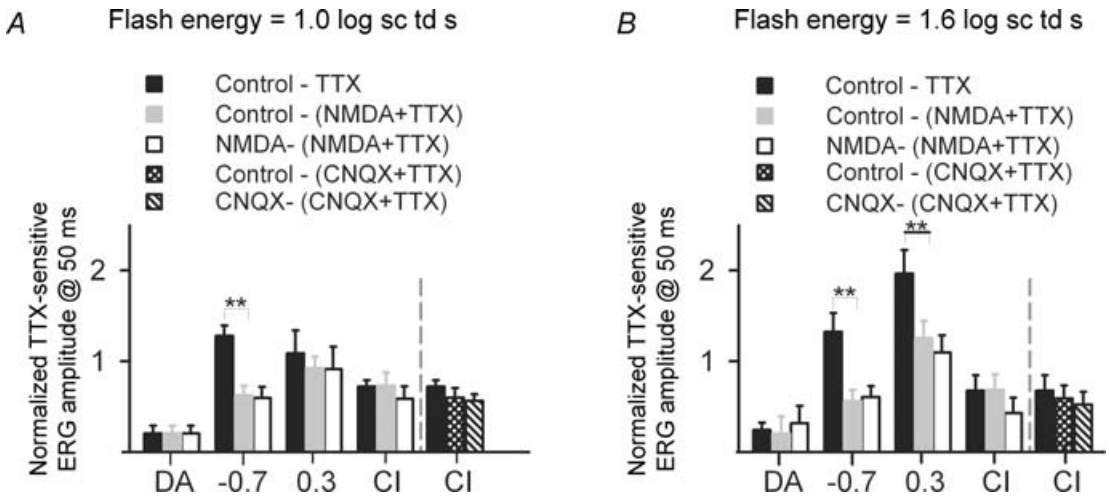

Figure 14. ERGs following suppression of inner retinal activity and TTX
Normalized TTX-sensitive ERG (group mean ± S.E.M.; same data set as in Fig. 4) measured at 50 ms (black bars: (Before TTX – After TTX)/Before TTX) and NMDA + TTX-sensitive (grey bars: (Before injection – After NMDA + TTX)/Before injection). Responses to two flash energies, 1.0 log sc td s (left) and 1.6 log sc td s (right) are shown. The TTX-sensitive response after NMDA also was normalized to the response after NMDA (white bars). On the far right of both graphs, CNQX results ($n = 6$) are shown for the dark-adapted cone-isolated (CI) condition (black bar: (Before TTX – After TTX)/Before TTX), CNQX + TTX-sensitive (cross-hatched bar: (Before injection – After NMDA + TTX)/Before injection) and the TTX-sensitive response after CNQX normalized to the response after CNQX (hatched bar). The CNQX data have been re-analysed from a previous study (Mojumder *et al.* 2007). For the NMDA studies, for dark-adapted conditions, $n = 8$ eyes; for −0.7 log sc td, $n = 4$; for 0.3 log sc td, $n = 5$; and for CI, $n = 4$). ** Statistically significant difference between TTX-sensitive and NMDA + TTX- or CNQX + TTX-sensitive ERG amplitudes (*t* test; $P < 0.05$).

occurred (at 9 weeks), ONTx did not affect the b-wave in the current study, or in the study of Li *et al.* (2005). ONTx also did not reduce the PhNR in the present study, although a reduction was reported after ONTx by Li *et al.* 2005). Bui & Fortune (2004) did not measure the PhNR. Although both the other studies examined a broader range of time points than in the present study, and effects on b-waves (Bui & Fortune, 2004) and PhNR (Li *et al.* 2005) were greater at later times (e.g. 9 weeks), all three studies made recordings around 4 weeks after ONTx. At that time point, the disparity in findings was still in evidence, but reduced, suggesting a possible role for time of recording after ONTx in producing different results across studies.

It is also possible that the disparate outcomes were due in part to differences in surgical approach. Aside from subtle differences that are not easily identified, two differences are evident. First, in our study, the globe was not touched; the optic nerve was approached via a perilacrimal route. In both of the other studies the optic nerve was approached via a subconjunctival route that involved a downward rotation of the eyeball. (The rotation also occurred in incomplete sham surgeries on fellow eyes in Bui & Fortune, 2004). Second, the optic nerve was transected at 2 mm from the globe in our study and that of Li *et al.* (2005), whereas it was cut closer to the globe (0.5–1 mm) by Bui & Fortune (2004) which would have led to slightly faster retrograde effects in the eye, the consequence of which is unknown.

Aside from the time of recording, and surgical approach, there were several methodological differences among the studies. Each study used electrodes made of different materials, and in our study and that of Li *et al.* (2005) recordings were made differentially between the eyes, with one eye covered, whereas Bui & Fortune (2004) referenced to a scleral conjunctival ring in the same eye and recorded from both eyes at once. Different stimulators were used in each study. Our study and that of Li *et al.* (2005) used narrow band LEDs, whereas Bui & Fortune (2004) used a white xenon flash. It is unclear whether these differences had impact on the findings.

Because the PhNR was reduced in monkeys following experimental glaucoma that damages the retinal ganglion cells (Viswanathan *et al.* 1999), as well as in human patients with open angle glaucoma, and other disorders affecting axons of ganglion cells (e.g. Viswanathan *et al.* 2001; Rangaswamy *et al.* 2004), our results indicate an interspecies difference. Primates may a have larger representation of the activity of ganglion cells and their axons in the flash ERG than rodents because of the greater number of ganglion cells, and their relatively higher density in the central retina. The PhNR in mice also appears to be more amacrine than ganglion cell related (LJ Frishman, unpublished observations). An amacrine cell origin in rodents is supported by loss of the response following injection of iontropic glutamate receptor antagonists such as PDA, CNQX and DNQX. TTX findings are supportive as well, although reductions in PhNR due to reduced input from cone bipolar cells affected by TTX could contribute to reductions in amplitudes of responses generated in the inner retina.

Na_v channels in the rod bipolar cell of primary rod circuit do not contribute to the leading edge of the b-wave

Under dark-adapted conditions, TTX did not affect stimulus–response curves until past the first saturation of the leading edge of the pre-injected b-wave, when cones became active, as shown in Fig. 9*B*, strongly suggesting that the effects of TTX were on circuits mediated by cone, rather than rod, bipolar cells. As discussed below, for mesopic conditions even when rod-driven responses were reduced by TTX, it is unlikely that the affected rod signals were travelling in the 'primary' rod pathway. An effect of TTX on cone rather than rod bipolar cells is consistent with observations in single cell studies in rat (Pan & Hu, 2000; Ma *et al.* 2005).

The lack of effect of TTX on the b-wave generated by the primary rod circuit, except for weak stimuli eliciting STRs in normal retina, indicates that TTX-sensitive feedback mechanisms were not affecting rod bipolar cell responses to stimuli above about –2.0 log sc td s at least up to the time of the b-wave peak (110 ms). This requires some explanation because feedback to rod bipolar cells certainly occurs. A17 amacrine cells, the principal neurons that make reciprocal feedback onto rod bipolar cells, have functional Na_v channels. However, findings of electrophysiological studies in both cat and rat retina suggest that Na_v channel activity in A17 amacrine cells may not be important for reciprocal GABAergic feedback, but instead, for long range effects (cat: Ellias & Stevens, 1980; rat: Hartveit, 1999; but see Dong & Hare (2002) for evidence of GABAergic feedback effects on the dark-adapted b-wave in rabbit retina).

For the mesopic conditions, particularly for the background of −0.7 log sc td, injection of TTX reduced amplitudes of both rod- and cone-driven b-waves (Fig. 9). The effects of TTX on rod-driven responses under mesopic conditions were probably on cone bipolar cell-mediated circuits, i.e. on the 'second' rod circuit created by gap-junctional communication between rods and cones, although some effects on inner retinal circuitry affecting rod bipolar cells cannot be excluded. The second rod circuit is thought to carry rod signals when stimulus conditions have saturated rod bipolar cell responses, but not rod responses (e.g. Smith *et al.* 1986). ERGs recorded in Cx36 (–/–) mice show a loss of sensitivity of the b-wave at certain mesopic background levels (Guldenagel *et al.* 2001), most likely due to loss of functional gap junctions between rods and cones, and hence, loss of transfer of rod signals

to cone bipolar cells (Guldenagel *et al.* 2001; Maxeiner *et al.* 2005). Studies of Cx36 (–/–) mice in the same experimental setup as the rat experiments resported here indicate that lowest rate of photoisomerization per rod (about 30 $Rh^* s^{-1}$ per rod) that caused an abnormally large loss of b-wave sensitivity in the mouse eyes, was similar to that produced by the −0.7 log sc td background in the rat experiments (Saszik *et al.* 2002*a*). This supports the conclusion that the TTX effects were on circuits mediated by cone rather than rod bipolar cells.

Under dark conditions the b-wave was more prolonged after TTX (protracted trailing edge of the b-wave seen in Figs 1 and 2). For low and moderate energy stimuli, this could be due at least in part to loss of the nSTR. For high energy stimuli, reduction of the PhNR of the underlying cone-driven responses could be involved (see Fig. 8, 1.9 log sc td s). TTX blockade of inner retinal feedback mechanisms onto bipolar cells (as suggested by Dong & Hare, 2000, for rabbit retina) may have also contributed to the prolonged trailing edges of b-waves.

Increases in b-wave amplitude and delays in b-wave peak time due to TTX in response to weak and strong flashes have been reported for the rabbit ERG measured after a short period (5 min) of dark adaptation (Dong & Hare, 2000), as well as for dark-adapted rat ERG responses to low to moderate stimulus energies (Bui & Fortune, 2004) and in salamander (Awatramani *et al.* 2001). Despite the increases in peak amplitude, the leading edges of the b-waves were well aligned after TTX in the rabbit study, as also observed in the present study. The increase in the rabbit ERG b-wave amplitude occurred only at times later than the time to peak of the control b-wave. Although we did not see an elevation of the dark-adapted b-wave amplitude in most experiments even at later peak times, b-wave peak times were slightly delayed for moderate stimulus strengths (see Fig. 2), and occasionally the delayed peaks were elevated, as seen by Bui & Fortune (2004). For example, a slight elevation of the dark-adapted b-wave occurred for flash energies around –1.3 log sc td s, in Mojumder *et al.* (2007), their Fig. 9. It is not clear if species and/or adaptation conditions produced differences across studies.

A small increase in the leading edge of the photopic b-wave after intravitreal TTX has been observed in macaque monkey ERGs (Viswanathan *et al.* 1999; Rangaswamy *et al.* 2004, 2007). In contrast, cone-driven b-waves in the present study in rat were never increased, although under light-adapted conditions, such as those used in the macaque studies, reductions in amplitude were smaller than for dark-adapted cone-isolated responses (Figs 9 and 15), and TTX elevated the trailing edge of cone-isolated responses in rats (see Fig. 8 for high stimulus energies).

In monkeys where TTX eliminates the PhNR in the light-adapted ERG, it also removes an earlier negative-going potential with a time course similar to the rising edge of the b-wave, thereby elevating the b-wave (Viswanathan *et al.* 1999; Rangaswamy *et al.* 2004, 2007). The earlier negative potential is not present in the rat. It is possible in monkeys that removal of the negative potentials by TTX masked any reduction of b-wave amplitude that may have been present. Preliminary experiments in our laboratory indicate that the dark-adapted cone-isolated ERG b-waves in monkeys are reduced by TTX, consistent with the presence of Na_v channels in macaque cone bipolar cells like those recently described for other species.

Na_v channels in second-order neurons of the cone circuit contribute to the b-wave

Cone-isolation experiments that eliminated rod signals revealed strong effects of TTX on cone-driven b-waves. Effects were greatest under dark-adapted conditions and least under light-adapted conditions when cone signals were somewhat desensitized. Previous work using CNQX to block light-evoked responses of all second- and third-order postreceptoral neurons other than ON cone bipolar cells, suggested that Na_v channels in the ON cone bipolar cells themselves were contributing to the cone-isolated b-wave (Mojumder *et al.* 2007). Immunohistological evidence points to the presence of a subset of Na_v channel α-subunits in the outer plexiform layer of mouse, rat and rabbit retina that is not associated with photoreceptors or horizontal cells, suggesting their likely location in the dendritic compartment of bipolar cells in these species (Mojumder *et al.* 2007), as previous observed in fish by Zenisek *et al.* (2001).

TTX-sensitive sodium currents have been found in isolated human photoreceptors, most notably in rods (Kawai *et al.* 2001, 2005), but in a few cones as well, localized to the inner segments. Because photoreceptors hyperpolarize in response to light, whereas Na_v channels open when membranes depolarize, the photoreceptors were not likely to be involved in the observed TTX effects.

TTX-sensitive Na^+ currents have also been found in isolated mammalian horizontal cells (Ueda *et al.* 1992, in cats; Löhrke & Hofmann, 1994, in rabbits). Na_v α-subunits have been localized in immunolabelling studies to horizontal cells in rat, rabbit and mouse retina (Mojumder *et al.* 2007). TTX-sensitive Na^+ currents, if present in rat horizontal cells, are not likely to play a significant role in attenuating cone-isolated b-waves for the following reasons. First, cone-isolated dark-adapted b-waves, and TTX effects on b-waves were not significantly altered following injection of CNQX that would have blocked light-evoked horizontal cell activity (Mojumder *et al.* 2007). Second, dark-adapted horizontal cells are relatively depolarized, –35 mV in mammals (Massey & Miller, 1987) causing voltage-dependent inactivation of Na_v channels under the conditions in which the

dark-adapted cone-isolated ERGs were recorded. Finally, because horizontal cells hyperpolarize in response to light whereas activation of Na_v channels requires membrane depolarization, active Na_v channels in horizontal cells could not affect the leading edge of the b-wave up to its peak.

Müller cell currents can contribute to the b-wave (Miller & Dowling, 1970; for review, see Frishman, 2005). However, light-evoked activity of Na_v channels in Müller cells, even if present in rats (and currently not confirmed, Chao *et al.* 1997), is unlikely to contribute to the b-wave. Resting Müller cell membrane potentials are quite hyperpolarized (around –85 mV, Miller & Dowling, 1970); their light-evoked voltage excursion is around 15 mV (in salamander; Miller & Dowling, 1970) whereas the activation threshold for Na_v channels is around –45 to –50 mV or maybe –60 mV (see below) making contributions unlikely (see also Dong & Hare, 2000).

Although our results using the ERG point to a significant role for Na_v channels in ON cone bipolar cells in controlling b-wave amplitude, they do not allow us to determine which types of ON bipolar cells were involved. Work in salamander (Ichinose *et al.* 2005) and ground squirrel retinas (Saszik & DeVries, 2005) implicate the more transient bipolar cells, and this is an area for further study.

Contribution of Na_v channels in inner retinal neurons to the b-wave

Effects of TTX on the mixed rod–cone ERG were greatest when the mesopic background of −0.7 log sc td was present. Intravitreal injection of NMDA, used to suppress at least some inner retinal activity, substantially reduced the large effects of TTX on mixed rod–cone signals seen under mesopic conditions which added to those seen in cone-isolated ERGs (Fig. 14). Taken together, these results point to involvement of rod-driven Na_v channel activity in the inner retina under mesopic conditions. Ganglion cell activity has been observed to be extinguished in many cases within minutes after application of high doses NMDA (200 mM or greater) in the isolated rabbit retina (W. A. Hare, personal communication), but because retinal ganglion lesions did not reduce the b-wave amplitude, the relevant inner retinal neurons with TTX-sensitive Na_v channels in this study were probably amacrine cells. Not all amacrine cells in the rat retina have NMDA receptors (e.g. Boos *et al.* 1993), but the activity of some might also have been reduced by local release of GABA or glycine from amacrine cells that were depolarized by NMDA.

Amacrine cells, well known for their involvement in feedback inhibition onto bipolar cells, can also affect feedback indirectly by disinhibiting other amacrine cells involved in feedback (Roska *et al.* 1998; Dong & Hare, 2000; Eggers & Lukasiewicz, 2006). Perhaps this occurred after TTX was injected in our experiments. The result is puzzling though, because the inner retinal effects were limited to mesopic levels of adaptation. Rod signals travelling in the second rod pathway (via rod–cone gap junctions) might have created more inner retinal activity under low mesopic conditions than higher levels of adaptation that desensitized or saturated inner retinal circuits. Alternatively, perhaps a third rod circuit in which rods contact OFF- (or ON-) cone bipolar cells directly (Soucy *et al.* 1998; Tsukamoto *et al.* 2001, 2007) was involved. However, the OFF circuit, at least, is not known to contribute significantly to the passage of rod signals to ganglion cells in rats (Protti *et al.* 2005). Finally, the large slow negative wave that was induced by TTX injection under mesopic conditions appeared to be pulling the b-wave down (e.g. Figs 1 and 2). The slow negative wave is reminiscent of a Müller cell-mediated inner retinal response that occurs in the degenerating retinas of aged Royal College of Surgeons rats under dark- and light-adapted conditions, and can be removed by intravitreal injection of NMDA (Bush *et al.* 1995; Machida *et al.* 2008).

$GABA_c$ receptors mediate inhibition at both rod and cone bipolar cell axon terminals in the rat retina (Enz *et al.* 1996). Intravitreal injection of 1,2,5,6-tetrahydropyridin-4-yl methylphosphinic acid (TPMPA), a selective antagonist for $GABA_c$ receptors, produced a decline in b-wave amplitude under mesopic conditions as large as that observed for TTX (DK Mojumder & LJ Frishman, unpublished observations), suggesting related effects. However, TPMPA also reduces the dark-adapted b-wave over much of its response range (Kapousta-Bruneau, 2000; Möller & Eysteinsson, 2003), an effect not seen for TTX in the present study.

Augmentation of the amplitude of cone-driven b-waves by Na_v channels

The stimulus–response functions for cone-isolated b-waves, plotted on log–log scales in Fig. 9*A* showed a downward shift of the entire curve after TTX. Stated another way, the results indicate that in control conditions activity of Na_v channels boosted the cone-driven response over its entire operating range. This shift reflected an increase of the maximum saturated amplitude, as shown by the change in the hyperbolic fit parameter V_{max} (see Table 4), which suggests that the contribution of at least some of the channels occurred after the responses had saturated, placing the effects downstream of the input to the cells generating the b-wave.

The presence of active Na_v channels augmented not only the maximum saturated amplitude of the b-wave, but also the gain, as measured by the responsivity (V_{max}/E_0) as shown in Table 4. Given the effects of TTX over the whole operating range, activation of the Na_v channels must

have occurred around resting levels for the bipolar cells. Existing physiological evidence indicates that Na_v channels can remain constantly activated (Pan & Hu, 2000) for resting membrane potentials of mammalian bipolar cells that have been shown to occur between –60 and –25 mV in numerous species (Kaneko *et al.* 1989; Karschin & Wässle, 1990; Gillette & Dacheux, 1995; Berntson & Taylor, 2000; Euler & Masland, 2000). This could augment subthreshold depolarizing potentials in the bipolar cell dendrites and cell bodies (Zenisek *et al.* 2001). Na_v channels in bipolar cells are thought to be on the somato-dendritic compartment of those cells (e.g. Pan & Hu, 2000; Zenisek *et al.* 2001).

To determine the factor by which Na_v channels augmented b-wave V_{max} and responsivity, the percentage by which each each parameter increased from the TTX-blocked case, to the control case, was calculated. Figure 15, top, shows that under control conditions Na_v channels boosted the V_{max} of the cone-driven b-wave by almost 350% in the dark-adapted state; this reduced by about 1/3 to ∼250% in the photopic condition. Figure 15, bottom, shows that change in responsivity (K) was greater. Na_v channels increased K by about 410% in the dark-adapted state, and this reduced to less than half that amount in the photopic condition. Although the trend was not statistically significant across all backgrounds, comparisons for V_{max} and for K revealed statistically significant differences between the fully dark-adapted and the photopic conditions for both parameters (t test; $P > 0.05$). Both changes indicate that light-evoked activity of Na_v channels in cone pathways was more effective under dark-adapted conditions than under light-adapted conditions. The finding that responsivity changed more on average (although variability was large) than V_{max} suggests that some of the TTX effects could have occurred before the saturation of the response as well as afterward. Although the mechanisms and exact loci in cone bipolar cells for these phenomena are unclear, evidence from related previous studies in slice preparations in salamander indicates that TTX-sensitive sodium currents in cone-driven transient ON bipolar cells are larger in dark-adapted retinas than in light-adapted retinas (Ichinose & Lukasiewicz, 2007). Because dopamine receptor agonists (D1) also were found to decrease the TTX-sensitive Na_v channel currents in salamander bipolar cells (Ichinose & Lukasiewicz, 2007), it is possible that the effect of light adaptation on Na_v channels in the mammalian retina may be via a dopamine receptor and second messenger system. Similar effects of dopamine on Na_v channels were found in goldfish retinal ganglion cells (Hayashida & Ishida, 2004), where the authors suggested that D1 agonists and activators of protein kinase A can decrease the number of Na_v channels available for activation at resting membrane potentials.

Suppression of cone-driven signals in the dark-adapted condition

Under dark-adapted conditions, TTX reduced the amplitude of the cone-isolated b-wave more than that of the b-wave in the full rod–cone ERG (see Fig. 9). This indicates that the light-evoked activity of Na_v channels in the ON-cone bipolar cells that generate the dark-adapted b-wave were suppressed when rods were active. A suppressive rod–cone interaction has been previously described in horizontal cells of salamander and cat (Goldberg *et al.* 1983; Frumkes & Eysteinsson, 1987; Pflug *et al.* 1990). Because the suppression appears to occur both in horizontal and bipolar cells, a likely site for the suppressive interaction in mammals is the cone pedicle where rod signals enter via gap junctions (e.g. Schneeweis & Schnapf, 1995).

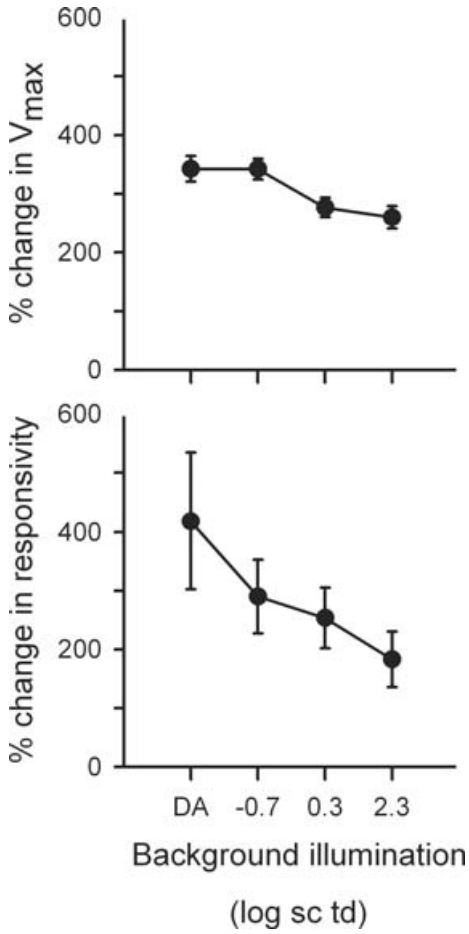

Figure 15. Effects of TTX on cone-isolated responses under different background conditions
Effects of TTX on V_{max} (top) and responsivity (bottom) of the fitted hyperbolic saturation function for cone-isolated ERG amplitudes measured at 50 ms before and after TTX. Error bars indicate ± S.E.M.

Summary

This study demonstrates in the rat retina, *in vivo*, Na_v channel activity that can be traced to cone pathways, even under dark-adapted conditions. Changing the level of adaptation from complete darkness to mesopic and photopic conditions leads to changes in the Na_v channel activity in cone bipolar cells, as well as in inner retinal circuits. A comparative study with other animals, coupled with more single cell investigations, may reveal a role for these sodium channels in their specific adaptive environments. Some pathologies are known to affect neuronal Na_v channels dramatically (for example, Dib-Hajj *et al.* 1999; Kamiya *et al.* 2004; Devaux & Scherer, 2005), and it may be important to consider this when evaluating ERGs in disease states. In addition to novel findings about the role of Na_v channels in retinal processing, the results reported in this paper represent an important step towards clarifying mechanistic interpretations of various wave components of the ERG, a non-invasive test of retinal function which is widely used in a broad range of applications.

References

Ahmed J, Frishman L & Robson JG (1999). Pharmacological removal of positive and negative STRs is required to isolate bipolar cell responses in the macaque scotopic electroretinogram. *Invest Opthalmol Vis Sci* **40** (Suppl.), S15.

Akula JD, Lyubarsky AL & Naarendorp F (2003). The sensitivity and spectral identity of the cones driving the b-wave of the rat electroretinogram. *Vis Neurosci* **20**, 109–117.

Awatramani G, Wang J & Slaughter MM (2001). Amacrine and ganglion cell contributions to the electroretinogram in amphibian retina. *Vis Neurosci* **18**, 147–156.

Berntson A & Taylor WR (2000). Response characteristics and receptive field widths of on-bipolar cells in the mouse retina. *J Physiol* **524**, 879–889.

Bignami A & Dahl D (1979). The radial glia of Muller in the rat retina and their response to injury. An immunofluorescence study with antibodies to the glial fibrillary acidic (GFA) protein. *Exp Eye Res* **28**, 63–69.

Birch DG, Hood DC, Locke KG, Hoffman DR & Tzekov RT (2002). Quantitative electroretinogram measures of phototransduction in cone and rod photoreceptors: normal aging, progression with disease, and test-retest variability. *Arch Ophthalmol* **120**, 1045–1051.

Björklund H, Bignami A & Dahl D (1985). Immunohistochemical demonstration of glial fibrillary acidic protein in normal rat Müller glia and retinal astrocytes. *Neurosci Lett* **54**, 363–368.

Bleakman D & Lodge D (1998). Neuropharmacology of AMPA and kainate receptors. *Neuropharmol* **37**, 1187–1204.

Boos R, Schneider H & Wässle H (1993). Voltage- and transmitter-gated currents of All-amacrine cells in a slice preparation of the rat retina. *J Neurosci* **13**, 2874–2888.

Bui BV & Fortune B (2004). Ganglion cell contributions to the rat full-field electroretinogram. *J Physiol* **555**, 153–173.

Bui BV & Fortune B (2006). Origin of electroretinogram amplitude growth during light adaptation in pigmented rats. *Vis Neurosci* **23**, 155–167.

Bush RA, Hawks KW & Sieving PA (1995). Preservation of inner retinal responses in the aged Royal College of Surgeons rat. Evidence against glutamate excitotoxicity in photoreceptor degeneration. *Invest Ophthalmol Vis Sci* **36**, 2054–2062.

Bush RA & Sieving PA (1994). A proximal retinal component in the primate photopic ERG a-wave. *Invest Ophthalmol Vis Sci* **35**, 635–645.

Calaza KC, de Mello FG & Gardino PF (2001). GABA release induced by aspartate-mediated activation of NMDA receptors is modulated by dopamine in a selective subpopulation of amacrine cells. *J Neurocytol* **30**, 181–193.

Celio MR, Baier W, Schärer L, Gregersen HJ, de Viragh PA & Norman AW (1990). Monoclonal antibodies directed against the calcium binding protein Calbindin D-28k. *Cell Calcium* **11**, 599–602.

Chao TI, Grosche J, Biedermann JB, Francke M, Pannicke T, Reichelt W, Wulst M, Muhle C, Pritz-Hohmeier S, Kuhrt H, Faude W, Drommer W, Kasper M, Buse E & Reichenbach A (1997). Comparative studies on mammalian Müller (retinal glial) cells. *J Neurocytol* **26**, 439–454.

Cohen ED (2001). Voltage-gated calcium and sodium currents of starburst amacrine cells in the rabbit retina. *Vis Neurosci* **18**, 799–809.

Cohen ED & Miller RF (1994). The role of NMDA and non-NMDA excitatory amino acid receptors in the functional organization of primate retinal ganglion cells. *Vis Neurosci* **11**, 317–332.

Dawson WW, Trick GL & Litzkow CA (1979). Improved electrode for electroretinography. *Invest Ophthalmol Vis Sci* **18**, 988–991.

Deans MR, Volgyi B, Goodenough DA, Bloomfield SA & Paul DL (2002). Connexin36 is essential for transmission of rod-mediated visual signals in the mammalian retina. *Neuron* **36**, 703–712.

Debus E, Weber K & Osborn M (1983). Monoclonal antibodies specific for glial fibrillary acidic (GFA) protein and for each of the neurofilament triplet polypeptides. *Differentiation* **25**, 193–203.

Devaux JJ & Scherer SS (2005). Altered ion channels in an animal model of Charcot-Marie-Tooth disease type IA. *J Neurosci* **25**, 1470–1480.

Dib-Hajj SD, Fjell J, Cummins TR, Zheng Z, Fried K, LaMotte R, Black JA & Waxman SG (1999). Plasticity of sodium channel expression in DRG neurons in the chronic constriction injury model of neuropathic pain. *Pain* **83**, 591–600.

Dixon RG & Eng LF (1980). Glial fibrillary acidic protein in the retina of the developing albino rat: an immunoperoxidase study of paraffin-embedded tissue. *J Comp Neurol* **195**, 305–321.

Dong CJ & Hare WA (2000). Contribution to the kinetics and amplitude of the electroretinogram b-wave by third-order retinal neurons in the rabbit retina. *Vision Res* **40**, 579–589.

Dong CJ & Hare WA (2002). GABAc feedback pathway modulates the amplitude and kinetics of ERG b-wave in a mammalian retina in vivo. *Vision Res* **42**, 1081–1087.

Dureau P, Bonnel S, Menasche M, Dufier JL & Abitbol M (2001). Quantitative analysis of intravitreal injections in the rat. *Curr Eye Res* **22**, 74–77.

Eggers ED & Lukasiewicz PD (2006). $GABA_A$, $GABA_C$ and glycine receptor-mediated inhibition differentially affects light-evoked signalling from mouse retinal rod bipolar cells. *J Physiol* **572**, 215–225.

Ellias SA & Stevens JK (1980). The dendritic varicosity: a mechanism for electrically isolating the dendrites of cat retinal amacrine cells? *Brain Res* **196**, 365–372.

Enz R, Brandstatter JH, Wassle H & Bormann J (1996). Immunocytochemical localization of the GABAc receptor rho subunits in the mammalian retina. *J Neurosci* **16**, 4479–4490.

Euler T & Masland RH (2000). Light-evoked responses of bipolar cells in a mammalian retina. *J Neurophysiol* **83**, 1817–1829.

Feigenspan A, Gustincich S, Bean BP & Raviola E (1998). Spontaneous activity of solitary dopaminergic cells of the retina. *J Neurosci* **18**, 6776–6789.

Friedburg C, Thomas MM & Lamb TD (2001). Time course of the flash response of dark- and light-adapted human rod photoreceptors derived from the electroretinogram. *J Physiol* **534**, 217–242.

Frishman LJ (2005). Electrogenesis of the ERG. In *Retina*, 4th edn, ed.Ryan SJ, pp. 103–113. Elsevier Mosby,

Frishman LJ, Reddy MG & Robson JG (1996). Effects of background light on the human dark-adapted ERG and psychophysical threshold. *J Opt Soc Am A Opt Image Sci Vis* **13**, 601–612.

Frishman LJ & Sieving PA (1995). Evidence for two sites of adaptation affecting the dark-adapted ERG of cats and primates. *Vision Res* **35**, 435–442.

Frumkes TE & Eysteinsson T (1987). Suppressive rod–cone interaction in distal vertebrate retina: intracellular records from *Xenopus* and *Necturus*. *J Neurophysiol* **57**, 1361–1382.

Gillette MA & Dacheux RF (1995). GABA- and glycine-activated currents in the rod bipolar cell of the rabbit retina. *J Neurophysiol* **74**, 856–875.

Goldberg SH, Frumkes TE & Nygaard RW (1983). Inhibitory influence of unstimulated rods in the human retina: evidence provided by examining cone flicker. *Science* **221**, 180–182.

Green DG & Powers MK (1982). Mechanisms of light adaptation in rat retina. *Vision Res* **22**, 209–216.

Guldenagel M, Ammermuller J, Feigenspan A, Teubner B, Degen J, Sohl G, Willecke K & Weiler R (2001). Visual transmission deficits in mice with targeted disruption of the gap junction gene connexin36. *J Neurosci* **21**, 6036–6044.

Hartveit E (1999). Reciprocal synaptic interactions between rod bipolar cells and amacrine cells in the rat retina. *J Neurophysiol* **81**, 2923–2936.

Haverkamp S & Wässle H (2000). Immunocytochemical analysis of the mouse retina. *J Comp Neurol* **424**, 1–23.

Hayashida Y & Ishida AT (2004). Dopamine receptor activation can reduce voltage-gated Na^+ current by modulating both entry into and recovery from inactivation. *J Neurophysiol* **92**, 3134–3141.

Hood DC & Birch DG (1990). The a-wave of the human electroretinogram and rod receptor function. *Invest Ophthalmol Vis Sci* **31**, 2070–2081.

Huber G & Matus A (1984). Immunocytochemical localization of microtubule-associated protein 1 in rat cerebellum using monoclonal antibodies. *J Cell Biol* **98**, 777–781.

Hughes A (1979). A schematic eye for the rat. *Vision Res* **19**, 569–588.

Ichinose T & Lukasiewicz PD (2007). Ambient light regulates sodium channel activity to dynamically control retinal signaling. *J Neurosci* **27**, 4756–4764.

Ichinose T, Shields CR & Luckasiewicz PD (2005). Sodium channels in transient retinal bipolar cells enhance visual responses in ganglion cells. *J Neurosci* **25**, 1856–1865.

Jacobs GH, Fenwick JA & Williams GA (2001). Cone-based vision of rats for ultraviolet and visible lights. *J Exp Biol* **204**, 2439–2446.

Johnson J, Tian N, Caywood MS, Reimer RJ, Edwards RH & Copenhagen DR (2003). Vesicular neurotransmitter transporter expression in developing postnatal rodent retina: GABA and glycine precede glutamate. *J Neurosci* **23**, 518–529.

Kamiya K, Kaneda M, Sugawara T, Mazaki E, Okamura N, Montal M, Makita N, Tanaka M, Fukushima K, Fujiwara T, Inoue Y & Yamakawa K (2004). A nonsense mutation of the sodium channel gene *SCN2A* in a patient with intractable epilepsy and mental decline. *J Neurosci* **24**, 2690–2698.

Kao CY (1966). Tetrodotoxin, saxitoxin and their significance in the study of excitation phenomena. *Pharmacol Rev* **18**, 997–1049.

Kapousta-Bruneau NV (2000). Opposite effects of $GABA_A$ and $GABA_C$ receptor antagonists on the b-wave of ERG recorded from the isolated rat retina. *Vision Res* **40**, 1653–1665.

Kawai F, Horiguchi M, Ichinose H, Ohkuma M, Isobe R & Miyachi E (2005). Suppression by an *h* current of spontaneous Na^+ action potentials in human cone and rod photoreceptors. *Invest Ophthalmol Vis Sci* **46**, 390–397.

Kawai F, Horiguchi M, Suzuki H & Miyachi E (2001). Na^+ action potentials in human photoreceptors. *Neuron* **30**, 451–458.

Kaneko A, Pinto LH, Tachibana M (1989). Transient calcium current of retinal bipolar cells of the mouse. *J Physiol* **410**, 613–629.

Karschin A & Wässle H (1990). Voltage- and transmitter-gated currents in isolated rod bipolar cells of rat retina. *J Neurophysiol* **63**, 860–876.

Kermer P, Klocker N, Weishaupt JH & Bahr M (2001). Transection of the optic nerve in rats: studying neuronal death and survival in vivo. *Brain Res Brain Res Protoc* **7**, 255–260.

Li B, Barnes GE & Holt WF (2005). The decline of the photopic negative response (PhNR) in the rat after optic nerve transection. *Doc Ophthalmol* **111**, 23–31.

Lipton SA & Tauck DL (1987). Voltage-dependent conductances of solitary ganglion cells dissociated from the rat retina. *J Physiol* **385**, 361–391.

Löhrke S & Hofmann HD (1994). Voltage-gated currents of rabbit A- and B-type horizontal cells in retinal monolayer cultures. *Vis Neurosci* **11**, 369–378.

Lyubarsky AL, Falsini B, Pennesi ME, Valentini P & Pugh EN Jr (1999). UV- and midwave-sensitive cone-driven retinal responses of the mouse: a possible phenotype for coexpression of cone photopigments. *J Neurosci* **19**, 442–455.

Lyubarsky AL, Lem J, Chen J, Falsini B, Iannaccone A & Pugh EN Jr (2002). Functionally rodless mice: transgenic models for the investigation of cone function in retinal disease and therapy. *Vision Res* **42**, 401–415.

Ma YP, Cui J & Pan ZH (2005). Heterogeneous expression of voltage-dependent Na^+ and K^+ channels in mammalian retinal bipolar cells. *Vis Neurosci* **22**, 119–133.

Machida S, Raz-Prag D, Fariss RN, Sieving PA & Bush RA (2008). Photopic ERG negative response from amacrine cell signaling in RCS rat retinal degeneration. *Invest Ophthalmol Vis Sci* **49**, 442–452.

Martin KR, Quigley HA, Zack DJ, Levkovitch-Verbin H, Kielczewski J, Valenta D, Baumrind L, Pease ME, Klein RL & Hauswirth WW (2003). Gene therapy with brain-derived neurotrophic factor as a protection: retinal ganglion cells in a rat glaucoma model. *Invest Ophthalmol Vis Sci* **44**, 4357–4365.

Massey SC & McGuire G (1998). The role of glutamate in retinal circuitry. In *Excitatory Amino Acids and Synaptic Transmission*, ed.Wheal HV & Thomson AM, pp. 201–221. Academic Press, London.

Massey SC & Miller RF (1987). Excitatory amino acid receptors of rod- and cone-driven horizontal cells in the rabbit retina. *J Neurophysiol* **57**, 645–659.

Massey SC & Miller RF (1990). *N*-Methyl-D-aspartate receptors of ganglion cells in rabbit retina. *J Neurophysiol* **63**, 16–30.

Maxeiner S, Dedek K, Janssen-Bienhold U, Ammermuller J, Brune H, Kirsch T, Pieper M, Degen J, Kruger O, Willecke K & Weiler R (2005). Deletion of connexin45 in mouse retinal neurons disrupts the rod/cone signaling pathway between AII amacrine and ON cone bipolar cells and leads to impaired visual transmission. *J Neurosci* **25**, 566–576.

Miller RF & Dowling JE (1970). Intracellular responses of the Muller (glial) cells of mudpuppy retina: their relation to b-wave of the electroretinogram. *J Neurophysiol* **33**, 323–341.

Miyachi E-I, Kawai F, Ohkuma M, Horiguchi M & Ichinose H (2006). Patch clamp analysis of voltage-gated Na^+ currents in human retinal bipolar cells. *Invest Ophthalmol Vis Sci* **47**, E-Abstract 3750.

Mojumder DK, Frishman LJ, Otteson DC & Sherry DM (2007). Voltage-gated sodium channel a-subunits $Na_v1.1$, $Na_v1.2$, and $Na_v1.6$ in the distal mammalian retina. *Mol Vis* **13**, 2163–2182.

Möller A & Eysteinsson T (2003). Modulation of the components of the rat dark-adapted electroretinogram by the three subtypes of GABA receptors. *Vis Neurosci* **20**, 535–542.

Naarendorp F, Sato Y, Cajdric A & Hubbard NP (2001). Absolute and relative sensitivity of the scotopic system of rat: electroretinography and behavior. *Vis Neurosci* **18**, 641–656.

Narahashi T, Moore JW & Scott WR (1964). Tetrodotoxin blockage of sodium conductance increase in lobster giant axons. *J Gen Physiol* **47**, 965–974.

Negishi K, Kato S & Teranishi T (1988). Dopamine cells and rod bipolar cells contain protein kinase C-like immunoreactivity in some vertebrate retinas. *Neurosci Lett* **94**, 247–252.

Nelson R (1977). Cat cones have rod input: a comparison of the response properties of cones and horizontal cell bodies in the retina of the cat. *J Comp Neurol* **172**, 109–135.

Nelson R, von Litzow A, Kolb H & Gouras P (1975). Horizontal cells in cat retina with independent dendritic systems. *Science* **189**, 137–139.

Nixon PJ, Bui BV, Armitage JA & Vingrys AJ (2001). The contribution of cone responses to rat electroretinograms. *Clin Experiment Ophthalmol* **29**, 193–196.

Nusinowitz S, Hood DC & Birch DG (1995). Rod transduction parameters from the a wave of local receptor populations. *J Opt Soc Am A Opt Image Sci Vis* **12**, 2259–2266.

Ohkuma M, Kawai F, Horiguchi M & Miyachi EI (2007). Patch-clamp recording of human retinal photoreceptors and bipolar cells. *Photochem Photobiol* **83**, 317–322.

Ostermann C, Dickmann U, Muley T & Mader M (1990). Large-scale purification of choline acetyltransferase and production of highly specific antisera. *Eur J Biochem* **192**, 215–218.

Pan ZH & Hu HJ (2000). Voltage-dependent Na^+ currents in mammalian retinal cone bipolar cells. *J Neurophysiol* **84**, 2564–2571.

Pasteels B, Rogers J, Blachier F & Pochet R (1990). Calbindin and calretinin localization in retina from different species. *Vis Neurosci* **5**, 1–16.

Paupoo AA, Mahroo OA, Friedburg C & Lamb TD (2000). Human cone photoreceptor responses measured by the electroretinogram *a*-wave during and after exposure to intense illumination. *J Physiol* **529**, 469–482.

Pflug R, Nelson R & Ahnelt PK (1990). Background-induced flicker enhancement in cat retinal horizontal cells. I. Temporal and spectral properties. *J Neurophysiol* **64**, 313–325.

Protti DA, Flores-Herr N, Li W, Massey SC & Wässle H (2005). Light signaling in scotopic conditions in the rabbit, mouse and rat retina: a physiological and anatomical study. *J Neurophysiol* **93**, 3479–3488.

Rangaswamy NV, Frishman LJ, Dorotheo EU, Schiffman JS, Bahrani HM & Tang RA (2004). Photopic ERGs in patients with optic neuropathies: comparison with primate ERGs after pharmacologic blockade of inner retina. *Invest Ophthalmol Vis Sci* **45**, 3827–3837.

Rangaswamy NV, Hood DC & Frishman LJ (2003). Regional variations in local contributions to the primate photopic flash ERG: revealed using the slow-sequence mfERG. *Invest Ophthalmol Vis Sci* **44**, 3233–3247.

Rangaswamy NV, Shirato S, Kaneko M, Digby BI, Robson JG & Frishman LJ (2007). Effects of spectral characteristics of ganzfeld stimuli on the photopic negative response (PhNR) of the ERG. *Invest Ophthalmol Vis Sci* **48**, 4818–4828.

Rangaswamy NV, Zhou W, Harwerth RS & Frishman LJ (2006). Effect of experimental glaucoma in primates on oscillatory potentials of the slow-sequence mfERG. *Invest Ophthalmol Vis Sci* **47**, 753–767.

Robson JG & Frishman LJ (1995). Response linearity and kinetics of the cat retina: the bipolar cell component of the dark-adapted electroretinogram. *Vis Neurosci* **12**, 837–850.

Robson JG & Frishman LJ (1996). Photoreceptor and bipolar-cell contributions to the cat electroretinogram: a kinetic model for the early part of the flash response. *J Opt Soc Am A Opt Image Sci Vis* **13**, 613–622.

Robson JG, Maeda H, Saszik SM & Frishman LJ (2004). In vivo studies of signaling in rod pathways of the mouse using the electroretinogram. *Vision Res* **44**, 3253–3268.

Robson JG, Saszik SM, Ahmed J & Frishman LJ (2003). Rod and cone contributions to the *a*-wave of the electroretinogram of the macaque. *J Physiol* **547**, 509–530.

Roska B, Nemeth E & Werblin FS (1998). Response to change is facilitated by a three-neuron disinhibitory pathway in the tiger salamander retina. *J Neurosci* **18**, 3451–3459.

Saszik SM & DeVries SH (2005). A TTX-sensitive Na^+-current in one type of ON bipolar cell in the ground squirrel retina. *Invest Ophthalmol Vis Sci* **46**, E-Abstract 1122.

Saszik SM, Frishman LJ & Paul D. (2002*a*). Effect of the rod-driven electroretinogram of eliminating Connexin-36 from the mouse retina. *Abstr Soc Neurosci* 236.8.

Saszik SM, Robson JG & Frishman LJ. (2002*b*). The scotopic threshold response of the dark-adapted electroretinogram of the mouse. *J Physiol* **543**, 899–916.

Schneeweis DM & Schnapf JL (1995). Photovoltage of rods and cones in the macaque retina. *Science* **268**, 1053–1056.

Sharma S, Ball SL & Peachey NS (2005). Pharmacological studies of the mouse cone electroretinogram. *Vis Neurosci* **22**, 631–636.

Shaw G & Weber K (1983). The structure and development of the rat retina: an immunofluorescence microscopical study using antibodies specific for intermediate filament proteins. *Eur J Cell Biol* **30**, 219–232.

Sherry DM, Mitchell R, Standifer KM & du Plessis B (2006). Distribution of plasma membrane-associated syntaxins 1 through 4 indicates distinct trafficking functions in the synaptic layers of the mouse retina. *BMC Neurosci* **7**, 54.

Sherry DM, Wang MM, Bates J & Frishman LJ. (2003*a*). Expression of vesicular glutamate transporter 1 in the mouse retina reveals temporal ordering in development of rod vs. cone and ON vs. OFF circuits. *J Comp Neurol* **465**, 480–498.

Sherry DM, Wang MM & Frishman LJ. (2003*b*). Differential distribution of vesicle associated membrane protein isoforms in the mouse retina. *Mol Vis* **9**, 673–688.

Sieving PA, Murayama K & Naarendorp F (1994). Push-pull model of the primate photopic electroretinogram: a role for hyperpolarizing neurons in shaping the b-wave. *Vis Neurosci* **11**, 519–532.

Skaliora I, Scobey RP & Chalupa LM (1993). Prenatal development of excitability in cat retinal ganglion cells: action potentials and sodium currents. *J Neurosci* **13**, 313–323.

Smith RG, Freed MA & Sterling P (1986). Microcircuitry of the dark-adapted cat retina: functional architecture of the rod-cone network. *J Neurosci* **6**, 3505–3517.

Soucy E, Wang Y, Nirenberg S, Nathans J & Meister M (1998). A novel signaling pathway from rod photoreceptors to ganglion cells in mammalian retina. *Neuron* **21**, 481–493.

Sugiyama K, Gu ZB, Kawase C, Yamamoto T & Kitazawa Y (1999). Optic nerve and peripapillary choroidal microvasculature of the rat eye. *Invest Ophthalmol Vis Sci* **40**, 3084–3090.

Thomas MM & Lamb TD (1999). Light adaptation and dark adaptation of human rod photoreceptors measured from the *a*-wave of the electroretinogram. *J Physiol* **518**, 479–496.

Toda K, Bush RA, Humphries P & Sieving PA (1999). The electroretinogram of the rhodopsin knockout mouse. *Vis Neurosci* **16**, 391–398.

Tsukamoto Y, Morigiwa K, Ishii M, Takao M, Iwatsuki K, Nakanishi S & Fukuda Y (2007). A novel connection between rods and ON cone bipolar cells revealed by ectopic metabotropic glutamate receptor 7 (mGluR7) in mGluR6-deficient mouse retinas. *J Neurosci* **27**, 6261–6267.

Tsukamoto Y, Morigiwa K, Ueda M & Sterling P (2001). Microcircuits for night vision in mouse retina. *J Neurosci* **21**, 8616–8623.

Ueda Y, Kaneko A & Kaneda M (1992). Voltage-dependent ionic currents in solitary horizontal cells isolated from cat retina. *J Neurophysiol* **68**, 1143–1150.

Viswanathan S, Frishman LJ & Robson JG (2000). The uniform field and pattern ERG in macaques with experimental glaucoma: removal of spiking activity. *Invest Ophthalmol Vis Sci* **41**, 2797–2810.

Viswanathan S, Frishman LJ, Robson JG, Harwerth RS & Smith EL 3rd (1999). The photopic negative response of the macaque electroretinogram: reduction by experimental glaucoma. *Invest Ophthalmol Vis Sci* **40**, 1124–1136.

Viswanathan S, Frishman LJ, Robson JG & Walters JW (2001). The photopic negative response of the flash electroretinogram in primary open angle glaucoma. *Invest Ophthalmol Vis Sci* **42**, 514–522.

Voigt T (1986). Cholinergic amacrine cells in the rat retina. *J Comp Neurol* **248**, 19–35.

Wachtmeister L (1998). Oscillatory potentials in the retina: what do they reveal. *Prog Retin Eye Res* **17**, 485–521.

Wang L, el Azazi M, Eklund A & Lillemor W (2001). Background light adaptation of the retinal neuronal adaptive system. I. Effect of background light intensity. *Doc Ophthalmol* **103**, 13–26.

Winsky L, Nakata H, Martin BM & Jacobowitz DM (1989). Isolation, partial amino acid sequence, and immunohistochemical localization of a brain-specific calcium-binding protein. *Proc Natl Acad Sci U S A* **86**, 10139–10143.

Xiang M, Zhou L, Macke JP, Yoshioka T, Hendry SH, Eddy RL, Shows TB & Nathans J (1995). The Brn-3 family of POU-domain factors: primary structure, binding specificity, and expression in subsets of retinal ganglion cells and somatosensory neurons. *J Neurosci* **15**, 4762–4785.

Xu L, Ball SL, Alexander KR & Peachey NS (2003). Pharmacological analysis of the rat cone electroretinogram. *Vis Neurosci* **20**, 297–306.

Xu X & Karwoski CJ (1994). Current source density analysis of retinal field potentials. II. Pharmacological analysis of the b-wave and M-wave. *J Neurophysiol* **72**, 96–105.

Zenisek D, Henry D, Studholme K, Yazulla S & Matthews G (2001). Voltage-dependent sodium channels are expressed in nonspiking retinal bipolar neurons. *J Neurosci* **21**, 4543–4550.

Acknowledgements

The authors thank Dr John G. Robson for comments on an earlier version of the document and Dr Adrian Glasser for his help with developing the optic nerve transection procedure. This work was supported by NIH Grants EY06671 (L.J.F.) and P30 EY07551 (UHCO).

Authors' present addresses

D. K. Mojumder: Verna and Marrs McLean Department of Biochemistry and Molecular Biology, Baylor College of Medicine, Houston, TX 77030, USA.

D. M. Sherry: University of Oklahoma Health Sciences Center, Department of Cell Biology, PO Box 26901, Oklahoma City, OK 73104, USA.

Supplemental material

Online supplemental material for this paper can be accessed at:
http://jp.physoc.org/cgi/content/full/jphysiol.2008.150755/DC1
and
http://www.blackwell-synergy.com/doi/suppl/10.1113/jphysiol.2008.150755